NREL/TP-411-5453 • UC Category: 271 • DE93010006

Continuous Roll-to-Roll a-Si Photovoltaic Manufacturing Technology

Semiannual Technical Progress Report 1 April 1992 – 30 September 1992

M. Izu
Energy Conversion Devices
Troy, Michigan

NREL technical monitor: R. Mitchell

National Renewable Energy Laboratory
1617 Cole Boulevard
Golden, Colorado 80401-3393
Operated by Midwest Research Institute
for the U.S. Department of Energy
under Contract No. DE-AC02-83CH10093

Prepared under Subcontract No. ZM-2-11040-7

April 1993

NOTICE

Printed in the United States of America
Available from:
National Technical Information Service
U.S. Department of Commerce
5285 Port Royal Road
Springfield, VA 22161

Price: Microfiche A01
Printed Copy A04

Codes are used for pricing all publications. The code is determined by the number of pages in the publication. Information pertaining to the pricing codes can be found in the current issue of the following publications which are generally available in most libraries: *Energy Research Abstracts (ERA)*; *Government Reports Announcements* and Index (*GRA* and I); *Scientific and Technical Abstract Reports (STAR)*; and publication NTIS-PR-360 available from NTIS at the above address.

Table of Contents

Preface

This Semi-Annual Technical Progress Report covers the work performed by Energy Conversion Devices, Inc. (ECD) for the period of April 1, 1992, to September 30, 1992, under DOE/NREL Subcontract number ZM-2-11040-7 entitled "Continuous Roll-to-Roll a-Si Photovoltaic Manufacturing Technology". The following personnel participated in the research program:

H. Bianchi
R. Ceragioli
J. Chema
A. Christian
B. Clark
R. Crucet
G. DeMaggio
X. Deng
B. Dotter
J. Evans
G. Hajatpoor
C. Harrison
R. Himmler
M. Izu
R. Kopf
A. Krisko
A. Kumar
M. Muller
A. Myatt
K. Narasimhan
H. Ovshinsky
S. Sullivan
D. Tsu
K. Whelan
R. Woz
R. Young

List of Figures

List of Figures
(continued)

List of Tables

Executive Summary

Objectives

The overall objective of this three-year program is to advance ECD's roll-to-roll, triple-junction photovoltaic manufacturing technologies, to reduce the module production costs, to increase the stabilized module performance, and to expand the commercial capacity utilizing ECD technology.

The specific three-year goal is to develop advanced large-scale manufacturing technology incorporating ECD's earlier research advances with the capability of producing modules with stable 11% efficiency at a cost of approximately $1.00 per peak watt.

Major efforts in the first year, Phase I, are the optimization of the high-performance back-reflector system, Task 1, the optimization of a-Si-Ge narrow band-gap solar cell, Task 2, and the optimization of the stable efficiency of the module, Task 3. Our goal is to achieve a stable 8% efficient 1ft. x 4ft. module. Also, the efforts include work on a proprietary, high deposition rate, microwave plasma, CVD manufacturing technology, Task 4, and on the investigation of material cost reduction, Task 5.

Summary

We have performed manufacturing technology development work utilizing our advanced continuous roll-to-roll triple-junction a-Si alloy solar cell production line, which was engineered and manufactured by ECD. The production line consists of:

1. A continuous roll-to-roll substrate washing machine.
2. A continuous roll-to-roll back-reflector machine.
3. A continuous roll-to-roll amorphous silicon alloy deposition machine.
4. A continuous roll-to-roll transparent conductor deposition machine.

The production line produces triple-junction two band-gap a-Si alloy solar cells consisting of Si/Si/Si-Ge structure on a 5 mil. thick, 14 in. wide, 2500 ft. stainless steel roll at a speed of 1ft./min. This production line represents the world's first commercial production line, which produces the most advanced high-efficiency amorphous Si alloy solar cells utilizing multi-junction spectrum-splitting cell design and high performance back-reflector.

In this six month program period, under Task 1, optimizing the back reflector system, we demonstrated for the first time that a high performance Ag/ZnOx back reflector can be incorporated into the production line.

The Ag/ZnOx back-reflector system has not been used previously in commercial modules because of its low production yield caused by shorts and shunts. By modifying the hardware design and optimizing process parameters to improve the quality of ZnOx layer and to eliminate mechanical defects, we have achieved a high production yield for the high performance Ag/ZnO back-reflector system.

Under Task 2 we have completed the initial optimization of Si-Ge alloy deposition parameters and demonstrated triple-junction solar cells having 38% quantum efficiency at

800nm. We have completed the initial improvements to the Si-Ge alloy deposition system by optimizing the deposition parameters, including the Ge content and the profile of Si-Ge composition.

Under Task 3 we have identified losses in ECD's 1ft. x 4ft. modules and reduced the shadow losses by redesigning grid/bus bar configurations.

The 1ft. x 4ft. modules that incorporated the high performance Ag/ZnO back-reflector, high quality Si-Ge layer, and improved grid/bus bar configurations have been produced.

The initial power output of a 1ft. x 4ft. module measured at ECD with a Spire Solar Simulator at 25°C was 33.7W. The initial module efficiency was measured to be 8.5% under standard conditions. The power output and efficiency of the same module measured at NREL using a Spire Solar Simulator were 34.2W and 8.56%, respectively. The stable efficiency after 500 hours light-soaking at approximately 50°C was 7%.

We have finished the hardware design of the microwave deposition system and are in the process of producing high quality a-Si layers, as per Task 4. We have identified and developed low-cost suppliers for germane and disilane in Task 5. The qualification analyses for these gases have been performed.

Major Accomplishments

- A high-performance Ag/metal oxide back-reflector system was successfully incorporated in our continuous roll-to-roll commercial production operation for the first time.

- For the first time, the high quality a-Si-Ge narrow band-gap solar cells have been incorporated in a commercial continuous roll-to-roll manufacturing.

- The world's first $4ft^2$ production PV modules utilizing triple-junction spectrum-splitting cell design have been produced in our commercial, continuous roll-to-roll production line.

- The initial aperture area efficiency of the $4ft^2$ module measured by NREL was 8.56%. The stable efficiency after 500 hours light-soaking at approximately 50°C was 7%. The stable efficiency is substantially higher than those of commercially available a-Si $4ft^2$ modules; typically 5 to 6%.

Milestones

	Phase I Milestones	Accomplishments
End of First Quarter		
m-1.1	Identify losses in present a-Si Alloy modules (Task 3)	Completed. 17% due to grid and bus-bar coverage, etching line loss.
m-1.2	Demonstrate stable representative >=4ft^2 a-Si Alloy module (Task 3)	Completed. η = 8.12% (ECD) η = 8.24% (NREL) Initial aperture area
End of Second Quarter		
m-1.3	Identify problems in Ag/ZnO back-reflector system (Task 1)	Completed. Low yield caused by mechanical defect.
m-1.4	Optimize metal/oxide back-reflector system (Task 1)	Completed.
m-1.5	Optimize metal/oxide back-reflector system (Task 1)	Completed.
m-1.6	Complete initial optimization of Si-Ge alloy deposition parameter for a 40% Quantum efficiency @ 800nm (Task 2)	Completed. QE=38% @ 800nm
m-1.7	Complete initial improvements to Si-Ge alloy deposition system (Task 2)	Completed.
m-1.8	Develop and qualify low-cost supplies for germane and disilane (Task 5)	Developed; Sovlux for germane and disilane; Initial tests completed. Require further testing.

Introduction

During the past ten years, ECD has made important progress in the development of materials, device designs, and manufacturing processes required for the continued advancement of practical photovoltaic technology[1-17]. Among these accomplishments, ECD has pioneered and continues further development of three key proprietary technologies, with significant potential for achieving the cost goals necessary for widespread growth of the photovoltaic market: (1) a low cost, roll-to-roll continuous substrate thin-film solar cell manufacturing process, (2) a high efficiency, monolithic, multiple-junction, spectrum-splitting thin-film amorphous silicon alloy device structure and (3) a high deposition rate, microwave plasma CVD process.

Commercial production of multiple-junction amorphous silicon alloy modules has been underway at ECD and its joint venture company for a number of years using ECD's proprietary roll-to-roll process and numerous advantages of this technology have been demonstrated. These include relatively low semiconductor material cost, relatively low process cost, a lightweight, rugged and flexible substrate that results in lowered installed costs of PV systems, and environmentally safe materials. Nevertheless, the manufacturing cost per watt of PV modules from our current plant remains high.

Under this Phase 2A Photovoltaic Manufacturing Technology (PVMAT) Program, ECD will advance its continuous roll-to-roll manufacturing technology and develop the capability of producing triple-junction multiple band-gap a-Si alloy photovoltaic modules with stable 11% efficiency at a cost of approximately $1.00 per watt in a high volume production plant. Major efforts will be focused on improving the stable efficiency of modules, increasing production throughput and reducing material and labor cost.

In order to achieve the high stable efficiency, ECD will develop and demonstrate large volume manufacturing technology that can incorporate earlier ECD research advances in device efficiency through the use of multi-junction spectrum-splitting and high performance back-reflector cell design. In this program period, Task 1: Optimization of the back-reflector system, Task 2: Optimization of the Si-Ge narrow band-gap solar cells, and Task 3: Optimization of the stable efficiency of photovoltaic modules, were directed towards achieving this goal.

We performed Task 2 and Task 3 in a continuous, roll-to-roll RF-plasma CVD processing system that produces, in a single pass, sequentially deposited thin films of doped and undoped amorphous silicon alloy semiconductors. Figure 1 illustrates the structure of a triple-junction spectrum-splitting solar cell produced using the processing system. Mixtures of feed-stock gases are decomposed at a pressure of approximately one Torr in a series of RF CVD plasma chambers to deposit amorphous alloy materials continuously on the coated stainless steel substrate. The multi-section amorphous silicon alloy deposition machine consists of a pay-off chamber section, nine process chamber sections, for the nine layers of the triple-junction solar cell and a take-up section. The process gas mixtures in each section are dynamically isolated from adjacent sections by proprietary "gas gates." The "gas gates" utilize laminar gas flow through constant geometrical cross section conduits in a direction opposite to the diffusion gradient of the dopant gas concentrations.

In this way, migration of dopants between chambers is essentially eliminated and gas mixtures in adjacent chambers are effectively isolated even though no actual physical impediment is present.

In Task 4 we are working to increase the production throughput. We report progress made in the area of high deposition rate amorphous silicon alloy solar cell deposition utilizing proprietary microwave plasma CVD technology.

In Task 5 we addressed a number of other issues that significantly reduce module cost including the reduction of the cost of gases utilized in our proprietary narrow-band-gap materials.

Figure 1: Structure of a triple-junction spectrum-splitting solar cell.

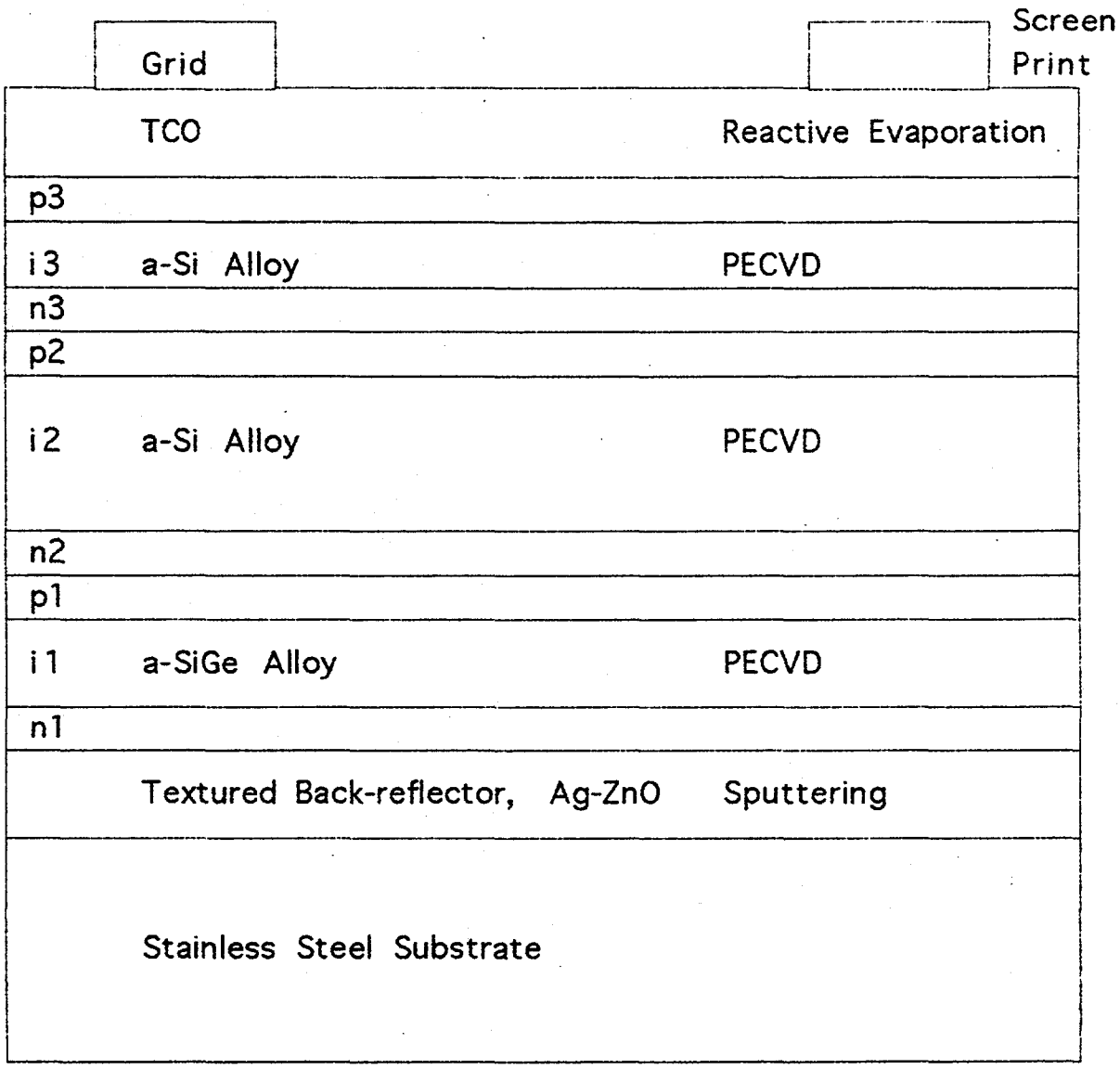

Task 1: Optimization of the Back-Reflector System

In our earlier manufacturing process, a textured Al alloy was used as a back-reflector. The high-efficiency research-scale device (we have demonstrated 13.7% efficiency, the world-record efficiency for a-Si alloy solar cell) utilized textured Ag/ZnO back-reflector that had a substantially higher reflectance and diffusiveness than the Al alloy back-reflector, resulting in an enhancement of Jsc in our laboratory cells. However, initial attempts to transfer this high-performance back-reflector technology to a manufacturing process had not been successful due to low yields. The object of this phase of our program has been focused on achieving the benefits of multiple internal reflections without suffering a reduction in yield due to shunting of the devices. We used Ag, in combination with ZnOx, in the back reflector. We improved the quality of Ag and ZnOx to improve the yield of the Ag/ZnO back reflector system.

Material and process optimizations were carried out using a roll-to-roll back-reflector production machine. The machine is equipped with, eight DC magnetron sputtering cathodes. Typically, two metal targets (adhesion promoting, and highly reflective metals such as, Cr, Al, and Ag) and six ZnO targets were loaded in the machine. The back-reflectors (Ag and ZnOx) were deposited sequentially at a speed of one foot per minute on a stainless steel roll that has a dimension of about 2500 ft., 14 in. wide, 5 mil thick. Ag, ZnOx system and Al/Ag, ZnOx system were deposited using the roll-to-roll back-reflector deposition production machine.

The yield and current provided by the back reflector was evaluated. This evaluation used our roll-to-roll a-Si and top-conductor machines as well as a research scale load-lock deposition system. The research scale deposition system has separate chambers for each doped layer and a-Si layer. It uses a RF parallel plate design and can deposit uniformly over approximately 2 in. x 2 in. area. A single n-i-p a-Si cell was deposited simultaneously on a standard back-reflector and on the Ag/ZnO back-reflector to be evaluated.

Preliminary testing showed that the sub-cell yield for Al/Ag, ZnOx was 96~100% while the sub-cell yield for the Ag, ZnOx system was 92~100%. However, the short circuit current for the Ag, ZnOx back-reflector system was 9.5% higher than the Al/Ag, ZnO system.

Sub-cell yield and gain in short circuit current were studied as a function of Ag thickness. Figure 2 shows an increase in Jsc as Ag thickness is increased, presumably due to enhanced internal reflection from a rougher morphology. However, we begin to see lower sub-cell yield for thicker Ag layers. We believe the yield is lower due to mechanical damage from rougher Ag produced as the layer is grown thicker.

Deposition conditions were adjusted for each layer of the Ag, ZnO system to optimize back-reflector microstructure. Deposition temperature, as well as Ag and ZnO layer thickness, and rate of sputtering, was found to affect film microstructure. The long wavelength region of the quantum efficiency curve shown in Figure 3 exhibits our

optimized diffuse reflection while Figure 4 shows our initial performance. Diffuse reflection exhibited by less evident interference fringes results in higher bottom-cell current as shown in Figure 3 and Figure 4. For the same Si:Ge cell, Figure 3 indicates 7.43 mA/cm^2 from the bottom cell while Figure 4 indicates only 6.78 mA/cm^2.

Causes for the low yield using the double-layered back-reflector system Ag, ZnOx have been investigated by structural/morphological/chemical analyses of the sites that caused shorts. We have determined that the shorts are caused by defects in the layer structure due to mechanical damage and foreign materials incorporated in the deposited layer during processing. Figure 5A shows mechanical damage, (i.e., cracking of the film). The cracks are due to dimples in the 5 mil stainless steel web created by metal particulates. Production machines and processes were improved to minimize particulate generation. Hence, shorts, due to the dimpling and film cracking, have been minimized to near zero.

Figure 5B shows a hole in the a-Si layer that results in a short. This pinhole was created when foreign material such as dust or particulate was transferred to the front side of the web, particularly before or during deposition of the a-Si layer. Low yield due to this type of pinholes has been minimized by implementing tight production procedures.

A high sub-cell yield (96~100%) has been achieved for Ag/ZnOx back-reflector systems after implementing the improvements in the machine and process. In summary, the high performance Ag/ZnO back-reflector system, has for the first time, been successfully incorporated in our continuous roll-to-roll production line.

Figure 2: **Plot of short-circuit current as a function of Ag thickness in back-reflector**

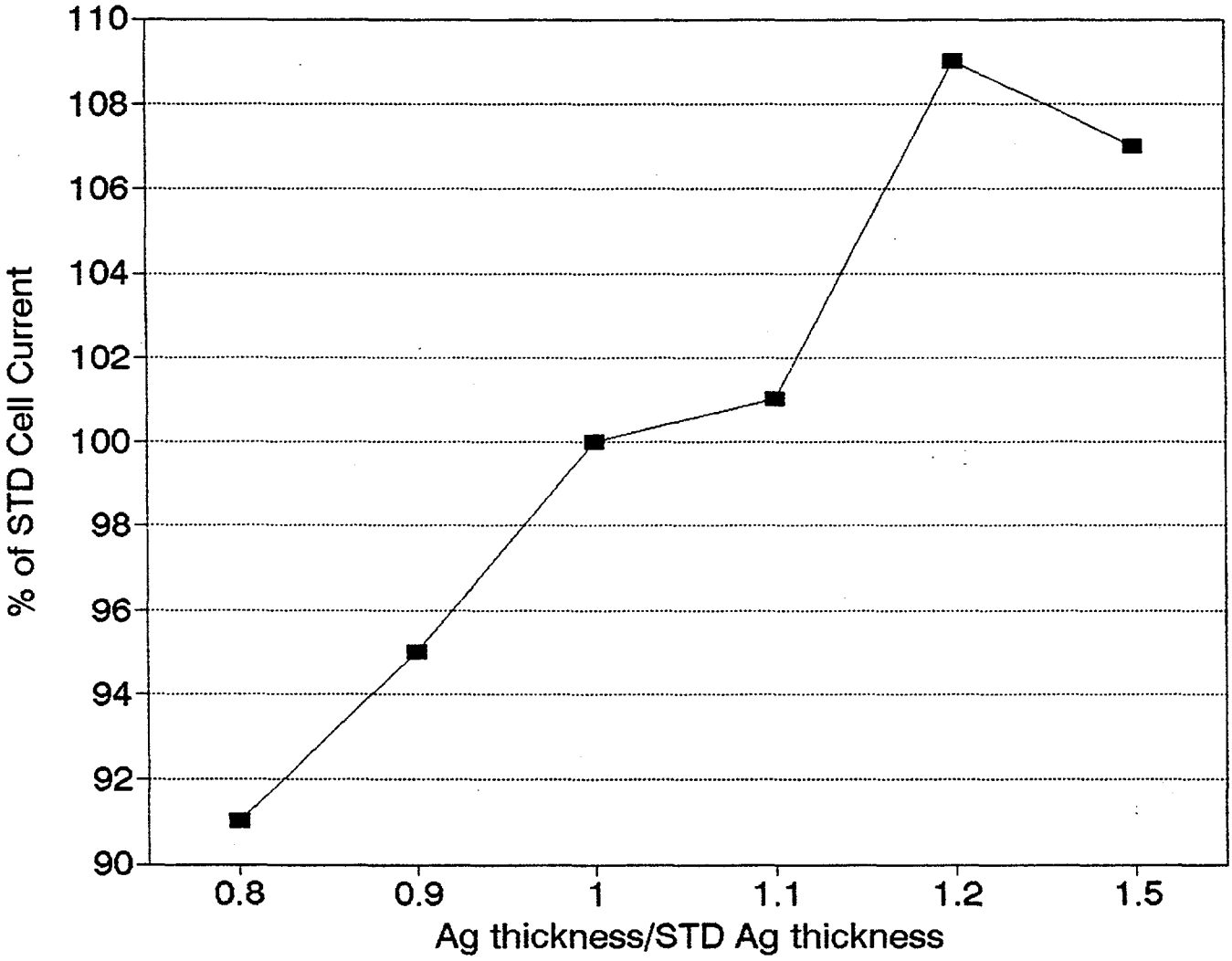

Figure 3: Quantum efficiency curve of a triple-junction solar cell having more textured back-reflector.

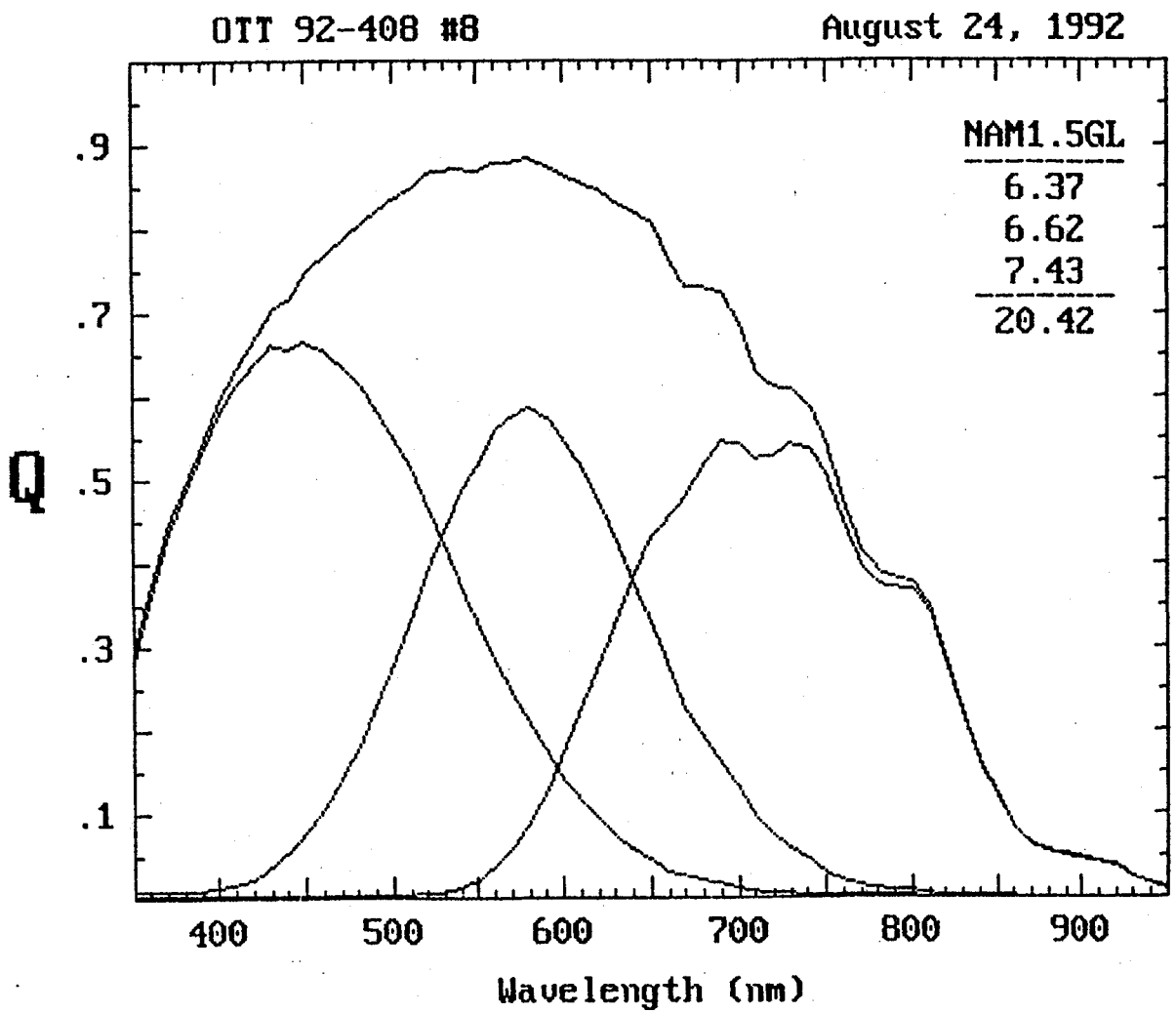

Figure 4: Quantum efficiency curve of a triple-junction solar cell having less textured back-reflector

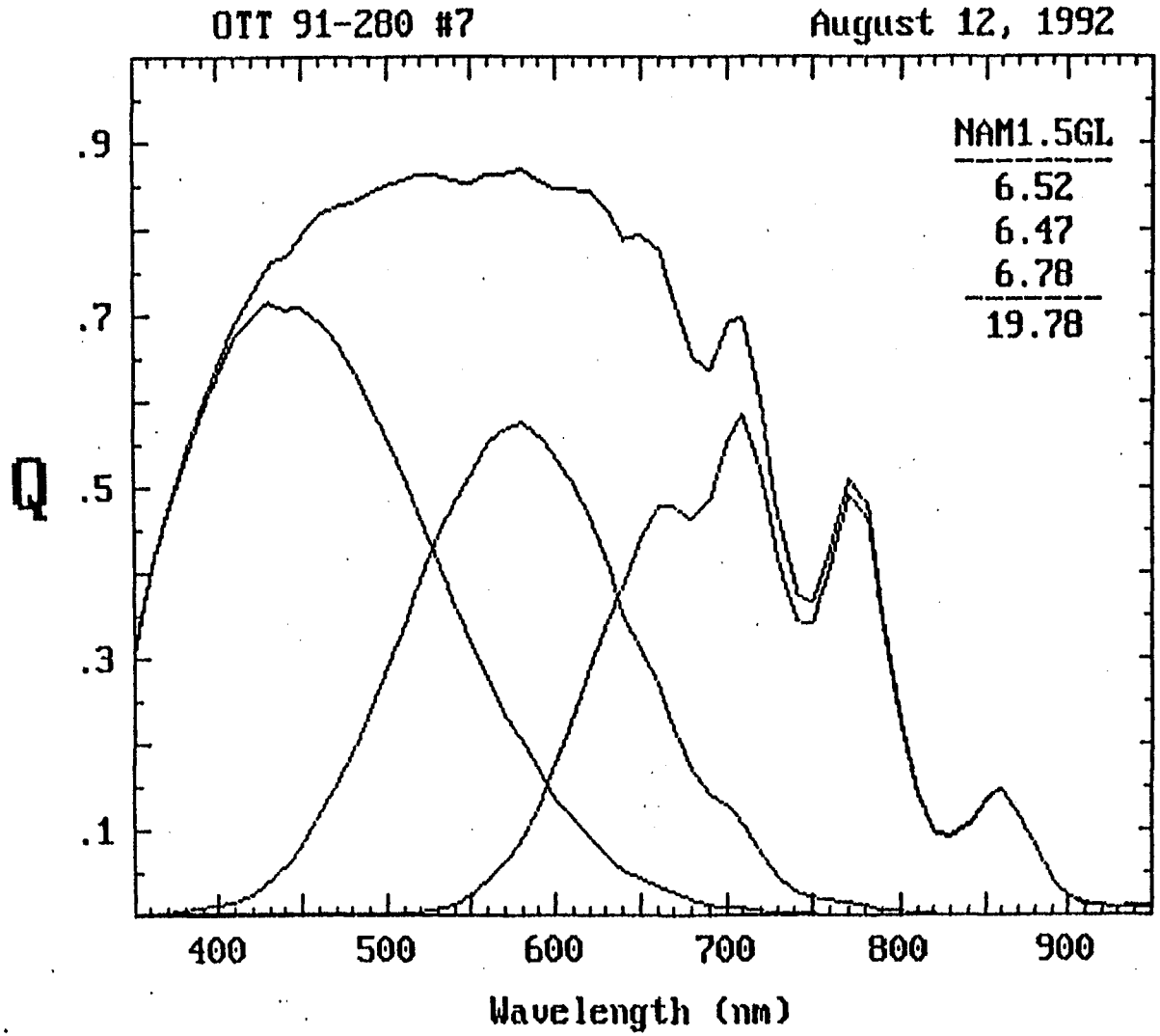

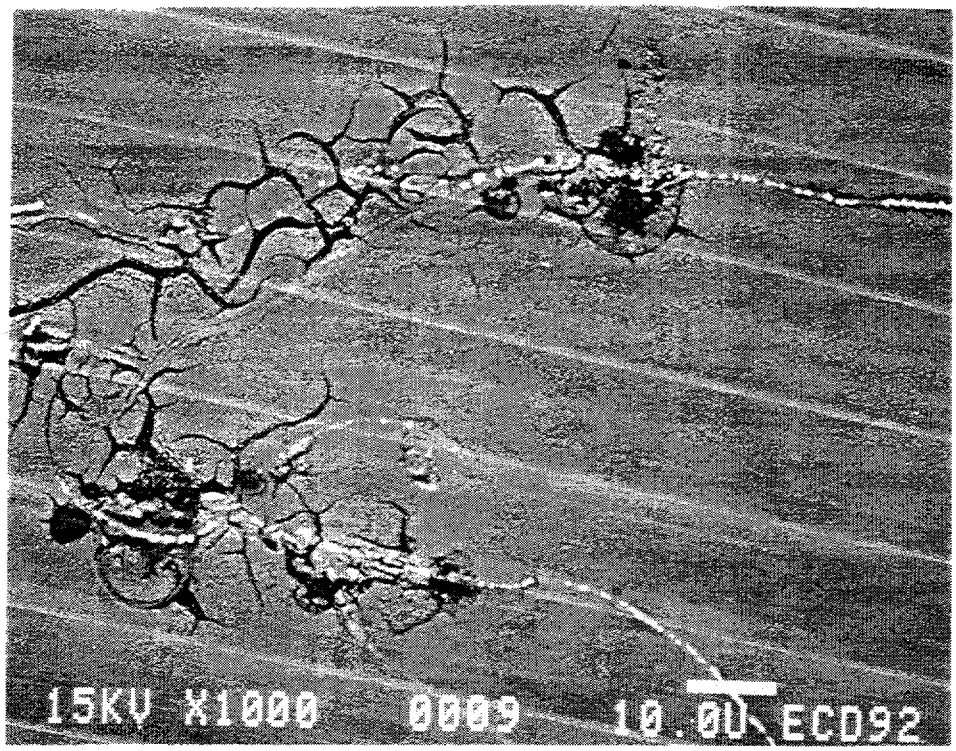

FIGURE 5A

Backscattering image of a triple junction solar cell showing mechanical damage

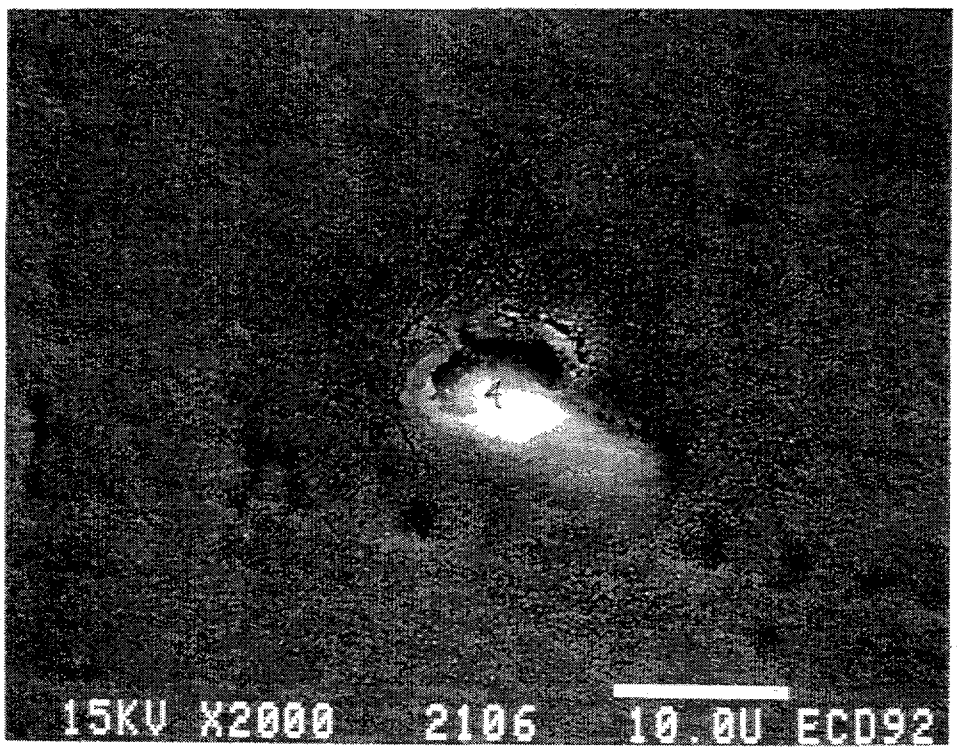

FIGURE 5B

A finished cell showing a hole present in a region of short.

Task 2: Optimization of the Si-Ge Narrow-Band-Gap Solar Cell

The a-Si-Ge narrow-band-gap bottom cell was deposited in our a-Si alloy roll-to-roll machine using RF glow discharge CVD on a moving stainless steel web coated with a back-reflector. This is the first time that an a-Si-Ge deposition process was incorporated into a continuous roll-to-roll production process. The bottom-cell section of the roll-to-roll process machine consists of three deposition chambers, an n1 chamber for the n^+ a-Si layer; a long i1 chamber for the a-Si-Ge layer; and a p1 chamber after i1, for the microcrystalline p^+ a-Si layer.

To increase the bottom cell performance, we profiled the bottom cell band-gap by changing the Ge content such that more light is absorbed near the p^+ junction to make hole collection easier. The graded band-gap induces an internal field to aid hole transport and hence improve the fill factor. The band-gap profiling is achieved in the roll-to-roll process utilizing specially designed proprietary gas distribution manifolds and cathode splitting.

The performance of a-Si-Ge bottom-cells depends on the Ge content, band-gap profile and the i layer thickness. We investigated such relations systematically using a-Si-Ge single-cell structure deposited on bare stainless steel in our roll-to-roll machine. We deposited a set of such cells with the same Ge content in the i layer but with different degrees of profiling. The fill-factor of the cell increased as the profile became steeper. Especially important is the increase in the fill-factor measured under red light, which is the light that a-Si-Ge cell sees as the bottom one of a triple-cell. When we further increased the degree of profiling, the loss in Voc became significant. We also studied the dependence of the bottom-cell on the Ge content but with a fixed profile. We covered the band gap from 1.4 to 1.6 eV. When the Ge content was increased, Jsc increased due to the smaller band gap. However, the losses in Voc and fill-factor became significantly large at a high Ge content. The loss in fill-factor is due to the increased defect density in the a-Si-Ge alloy at a high Ge content.

We optimized the Ge content, degree of band-gap profiling, and the thickness of the bottom cell i layer, based on the response of the cell under red illumination. Figure 6 shows the J-V characteristics of a typical single-junction Si-Ge cell deposited on Ag-ZnO back-reflector. Figure 7 shows the J-V measured under filtered blue and red light. The red fill-factor of this Si-Ge cell was 59%, as is seen in Figure 7. Figure 8 shows the quantum efficiency curve of this same cell. The relatively high red fill-factor and high response to the red suggests that this narrow-band-gap bottom-cell was well suited for use as the bottom-cell of triple-junction solar-cell.

We have studied the dependence of cell performance on the Ge content, band-gap profiling, and thickness inside a triple-junction solar cell structure. In Figure 9 and Figure 10 we show the J-V characteristics of two triple-junction cells with identical structures except that the bottom cell i layers have different Ge content, band-gap profiling and thickness. Sample 1, having a bottom cell i layer containing more Ge and with a steeper profile, shows a higher fill-factor due to higher current density from the bottom component cell under AM1.5 illumination. Sample 2, having a bottom cell i layer containing less Ge, with

less profile and being thicker, shows higher Voc. The efficiencies of these two cells are the same, indicating that there is a trade-off between Jsc and Voc. In Figure 11 and Figure 12, we show the quantum efficiency curves of Sample 1 and Sample 2. Although the bottom-cell of Sample 1 contributes relatively less Voc compared to that of Sample 2, it absorbs more light in the red and also, it has better fill-factor, hence it increases the overall fill-factor of the triple-cell.

Using the optimized a-Si-Ge bottom cell in our a-Si alloy roll-to-roll deposition machine, we achieved triple-junction solar-cell with 38% quantum efficiency, at wavelength of 800nm. Figure 13 is a quantum efficiency curve of a triple-junction cell using such optimized a-SiGe bottom cell. The fringes in the quantum efficiency curve are due to interference effect. We see from the figure that Q(800nm) = 0.38 (after smoothing out the interference fringes.)

We have demonstrated the production of high quality a-Si-Ge solar cells on 2500 ft. production rolls in a highly uniform and consistent manner in our continuous roll-to-roll amorphous silicon alloy deposition machine.

Figure 6: J-V Curve of a-Si-Ge single-cell deposited on Ag-ZnO back-reflector.

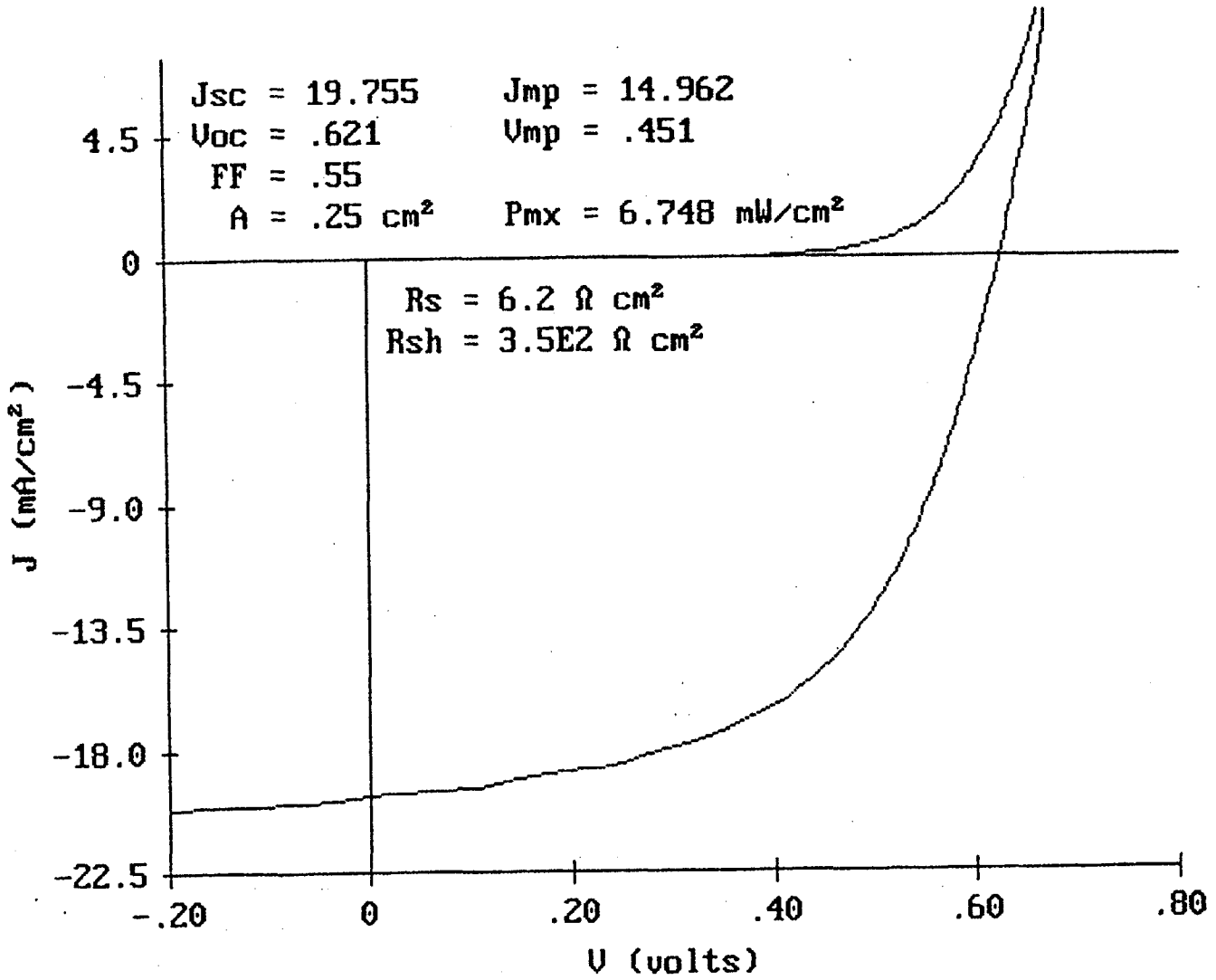

Figure 7: J-V Curve of a-Si-Ge single-cell measured under filtered blue and red light.

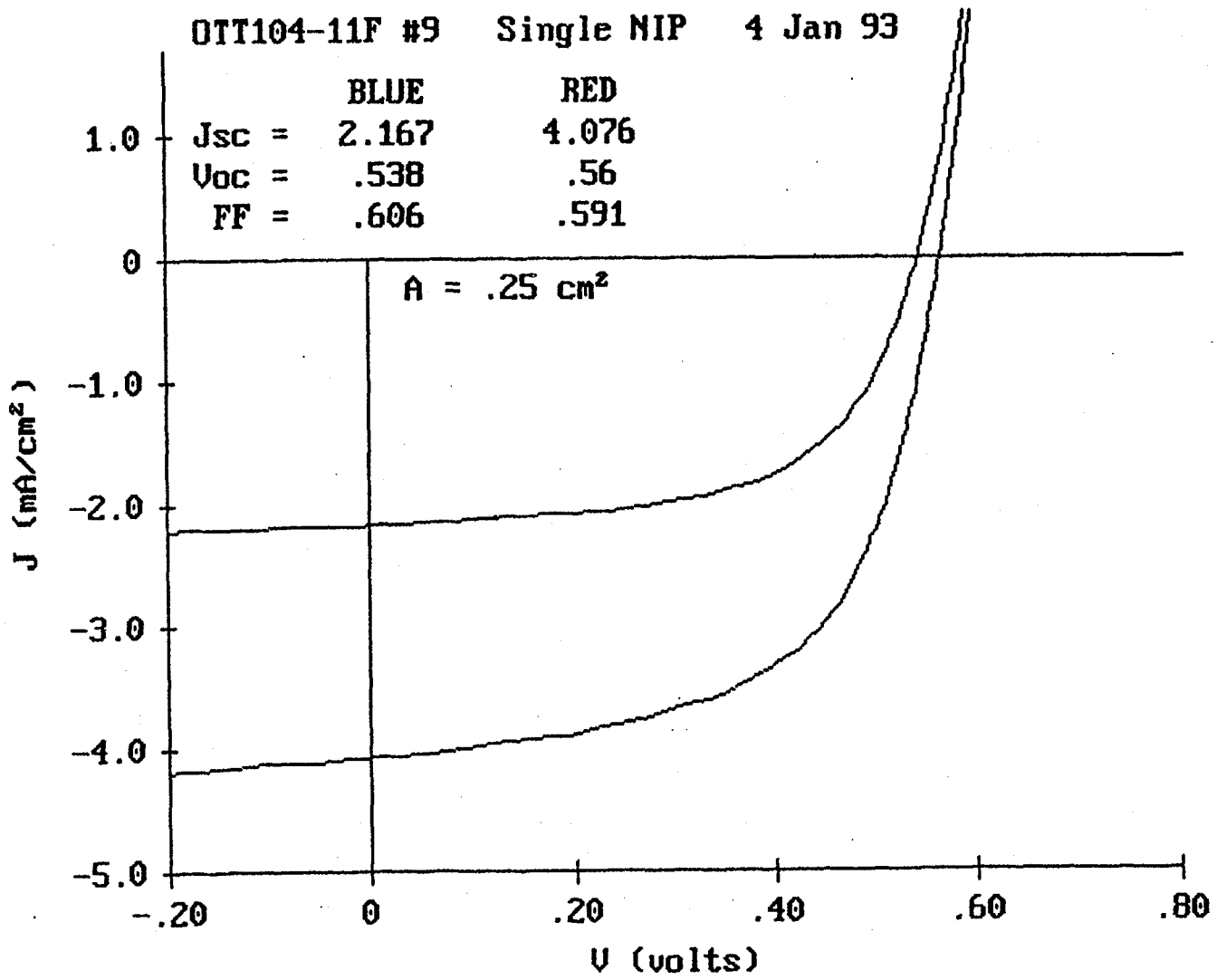

Figure 8: **Quantum efficiency curve for a-Si-Ge single-cell deposited on Ag-ZnO back-reflector.**

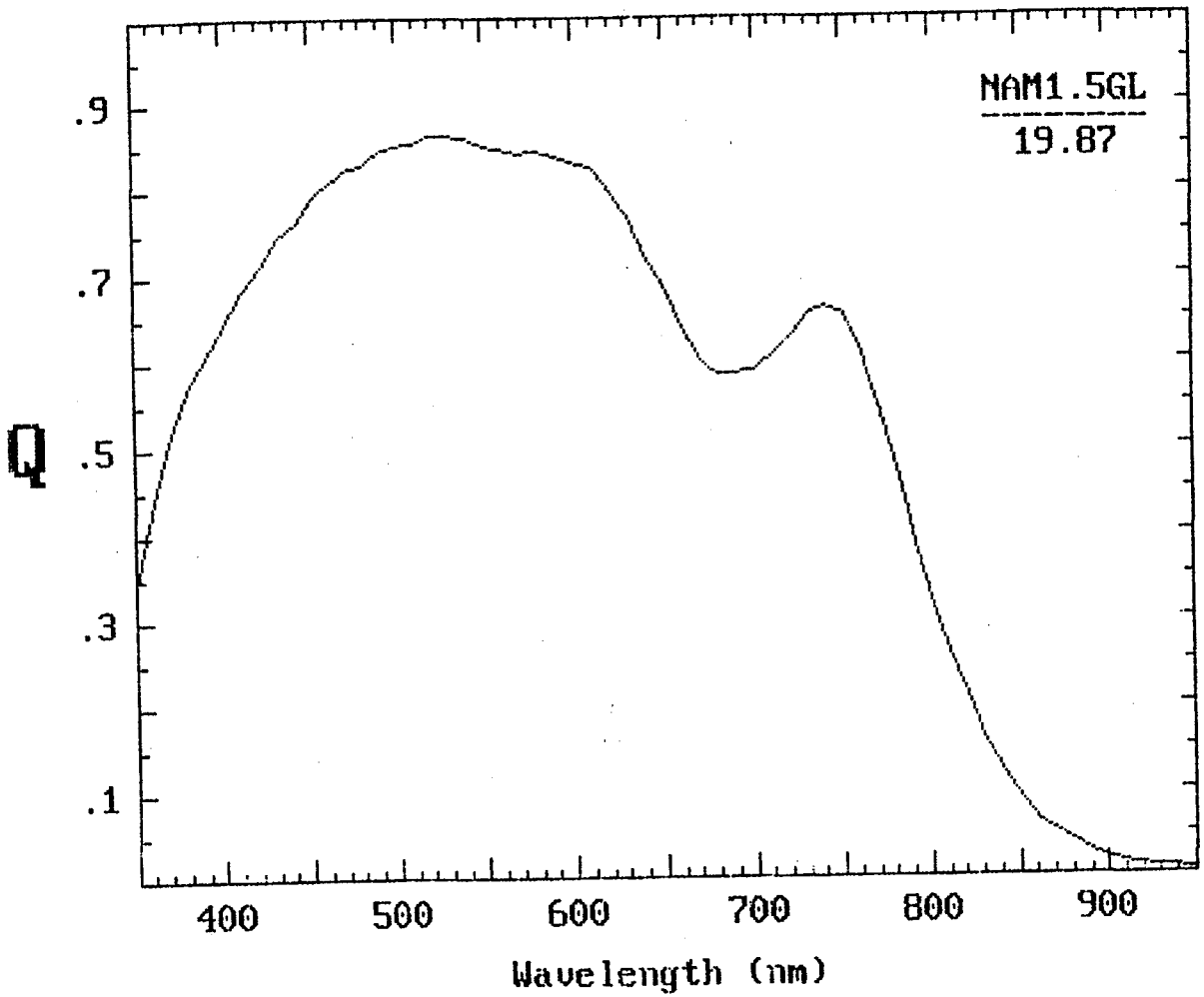

Figure 9: **J-V Curve of a triple-junction solar cell (sample 1) utilizing a-Si-Ge bottom-cell with relatively high Ge content.**

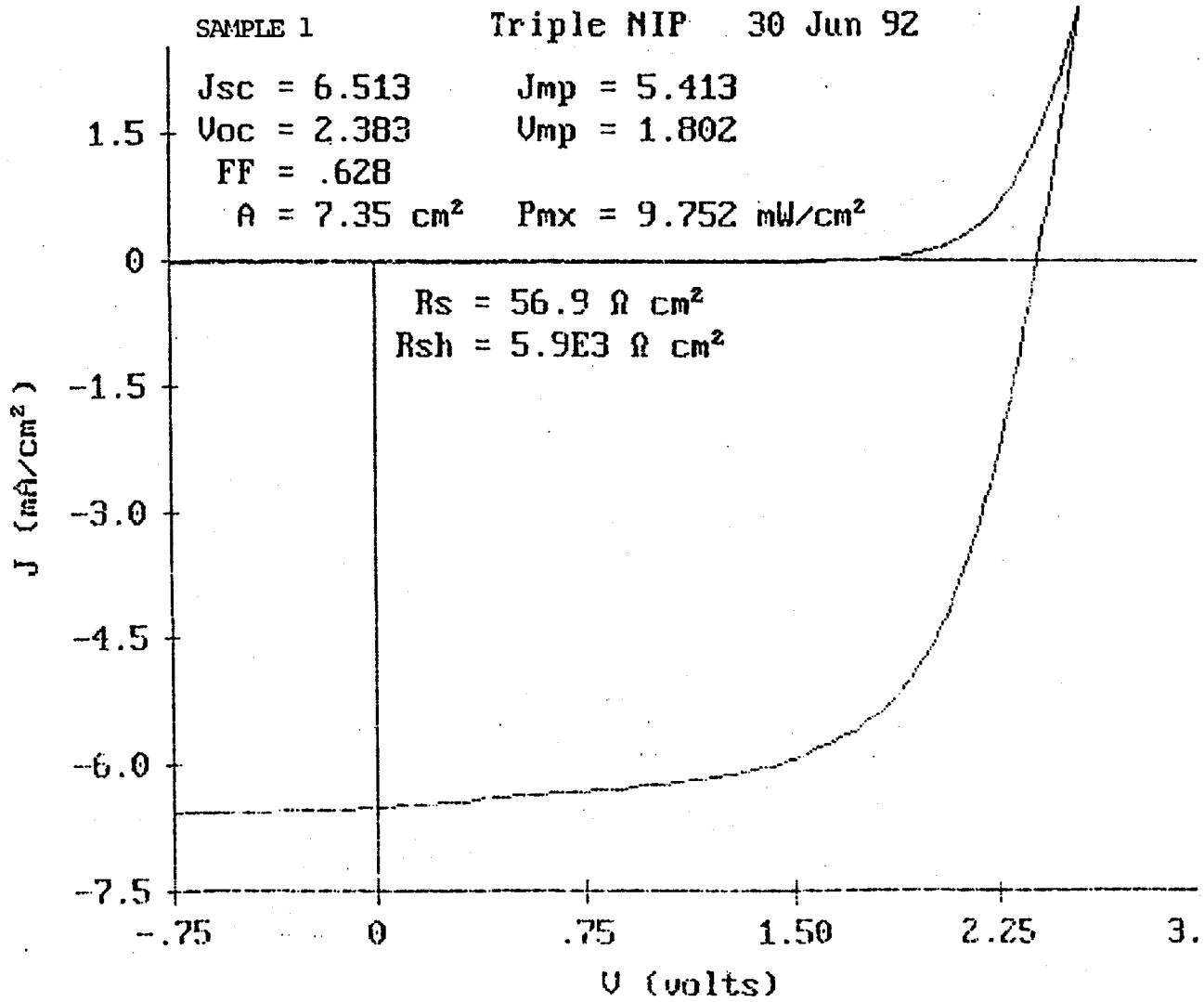

Figure 10: **J-V Curve of a triple-junction solar cell (sample 2) utilizing a-Si-Ge bottom-cell with relatively low Ge content.**

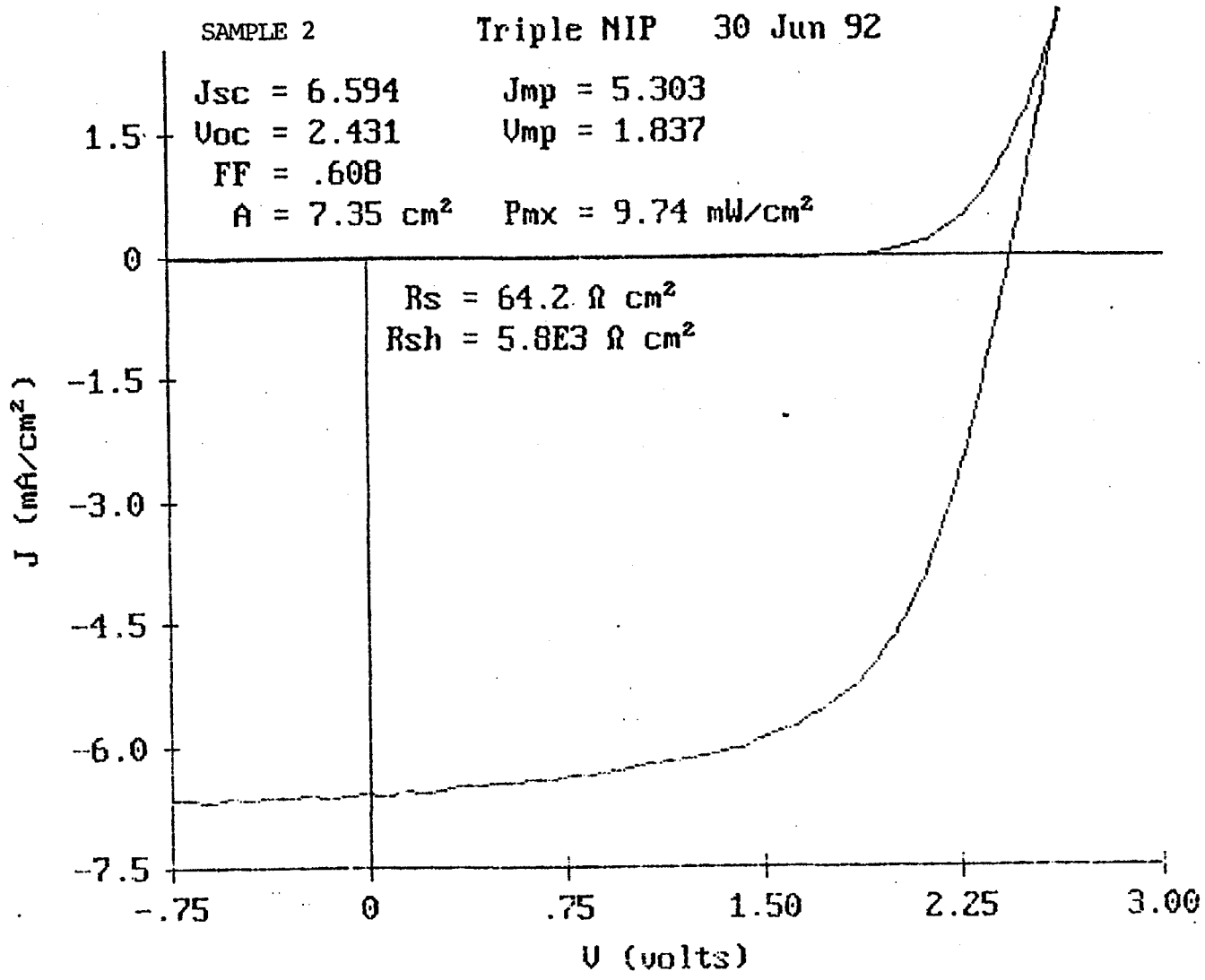

Figure 11: **Quantum efficiency curve of triple-junction solar cell sample 1.**

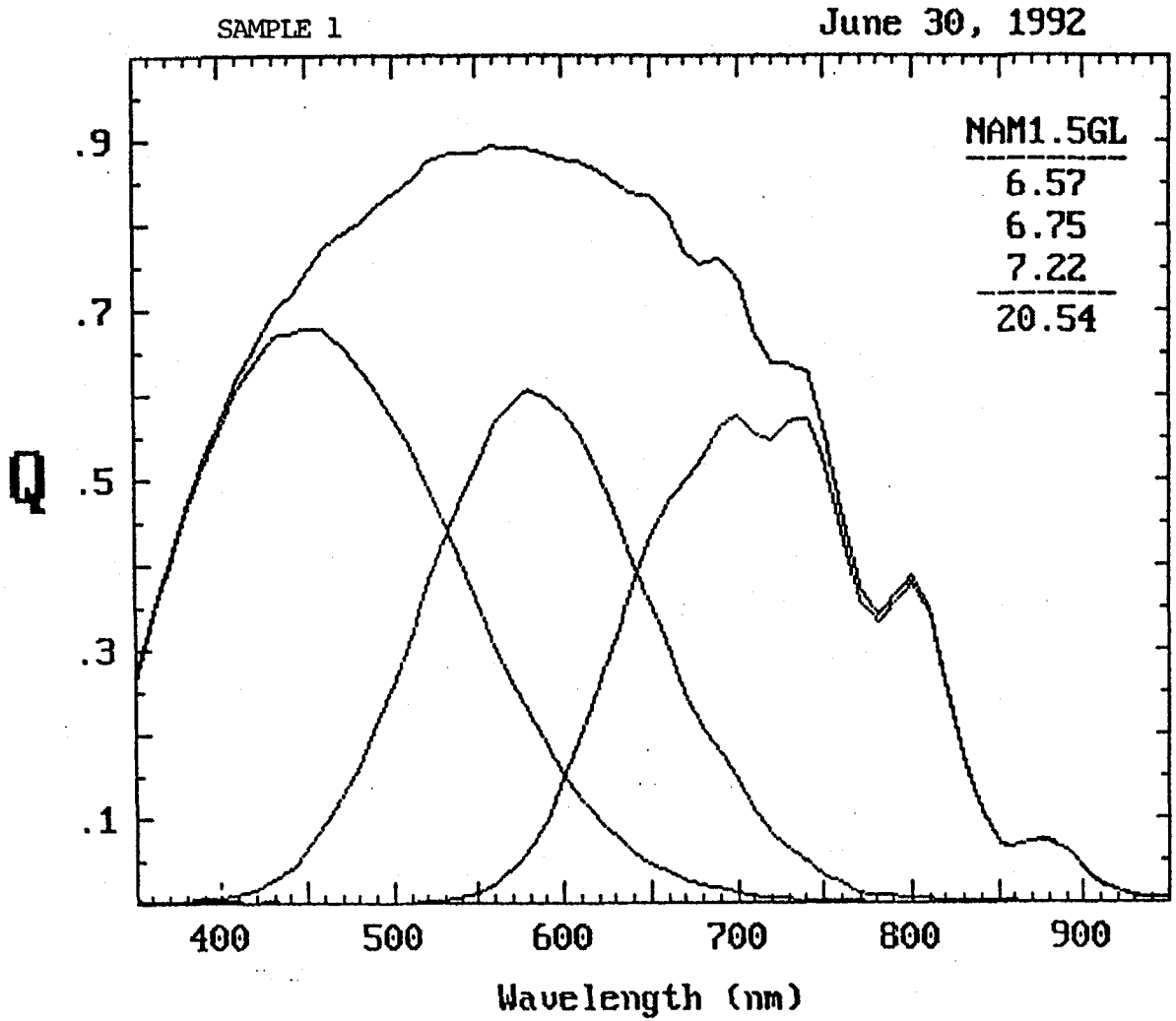

Figure 12: Quantum efficiency curve of triple-junction solar cell sample 2.

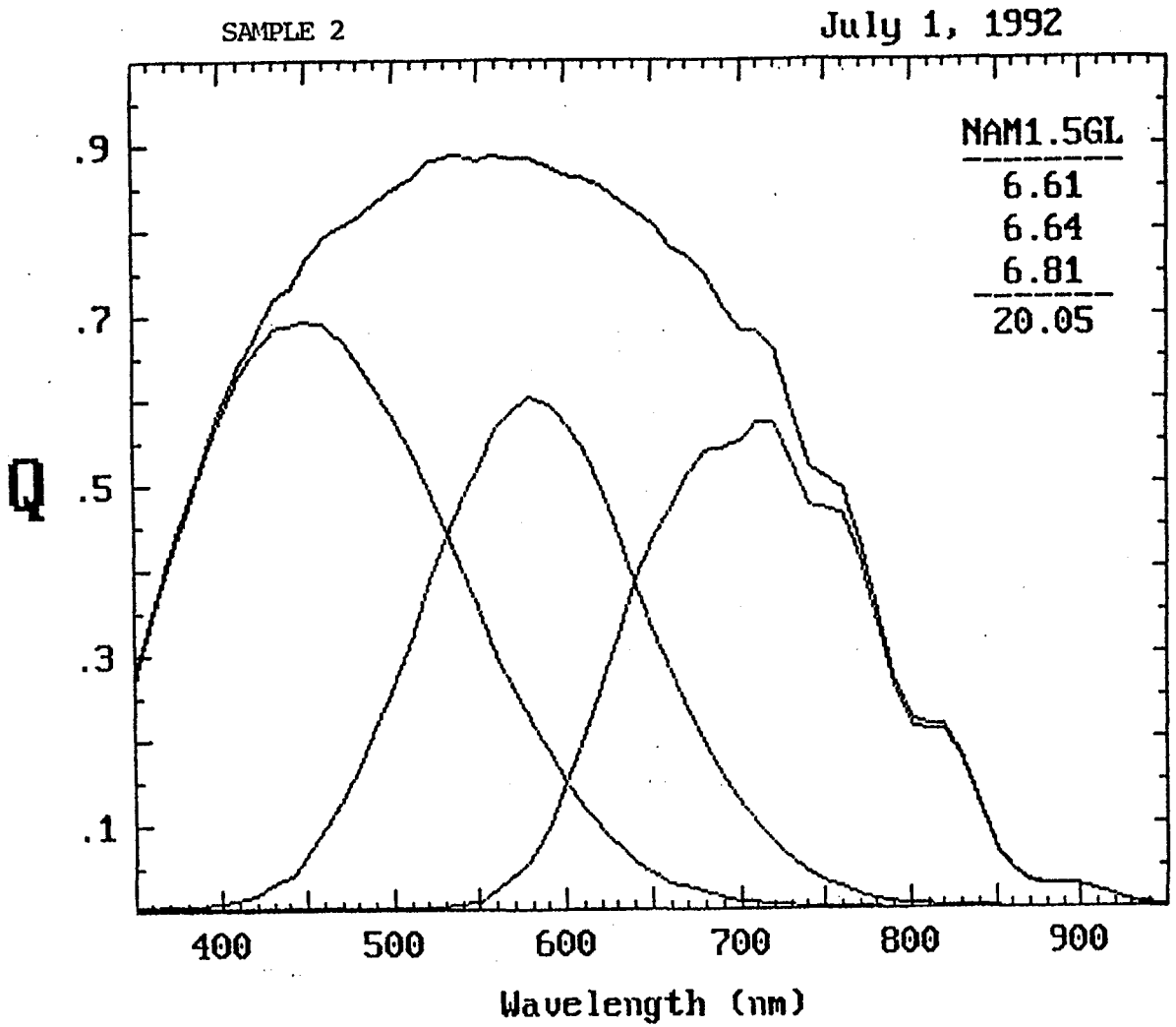

Figure 13: **Quantum efficiency curve for a triple-junction solar cell showing 38% quantum efficiency at 800nm.**

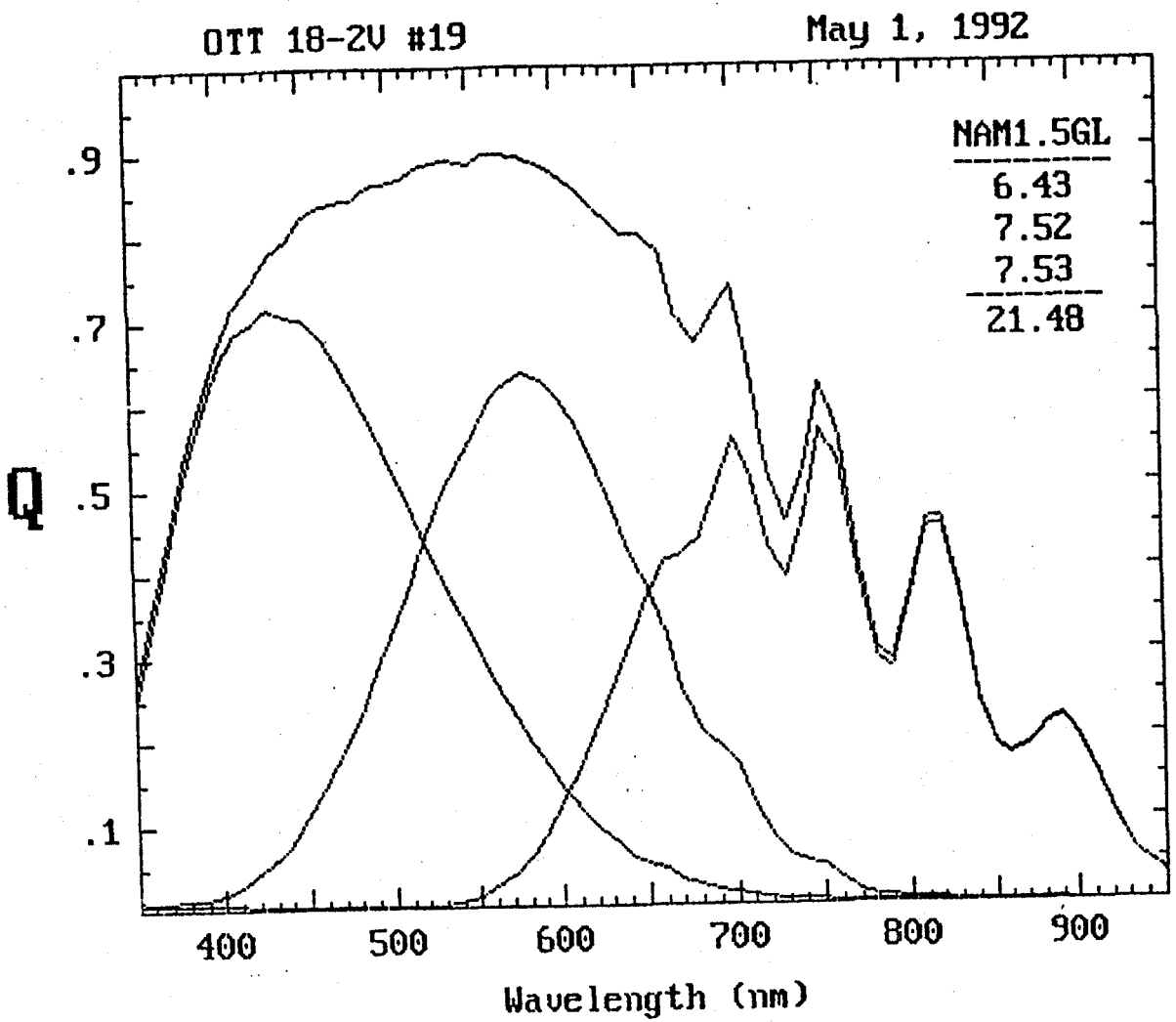

Task 3: Optimization of the Stable Efficiency of Photovoltaic Modules

General Manufacturing Process

The continuous roll-to-roll a-Si alloy solar cell production line consisting of a continuous roll-to-roll substrate washing machine, a continuous roll-to-roll back-reflector machine, a continuous roll-to-roll amorphous silicon alloy deposition machine, and a continuous roll-to-roll transparent conductive oxide deposition machine was used to optimize machine hardware design and process conditions for achieving the production of high-efficiency, stable a-Si alloy solar cells having Si/Si/Si-Ge triple cell structure. The production line was operated at 1ft. per minute. Rolls of 5 mil thick, 14 in. wide, 2500 ft. long stainless steel were used as the substrate. Pictures of the production plant and four roll-to-roll machines are shown in Figure 14 through Figure 18.

A processed solar cell roll was cut by a slab cutter typically into 48 in. long, 14 in. wide "slabs". Also, a certain number of 4 in. x 14 in. QA/QC coupons were cut from the rolls for QA/QC testing of the sections of the roll.

1ft. x 4ft. photovoltaic modules encapsulated with EVA/Tefzel polymers were assembled by processing the slabs in the following steps:

1. TCO Scribing
2. Short passivation
3. Screen print grid pattern
4. Final assembly
   - cell cutting
   - cell interconnect
   - laminating
   - module finishing
   - testing

The schematic drawing of a 1ft. x 4ft. module is shown in Figure 19.

Optimization of Solar Cell Performance

During this program, the entire process including substrate washing process, back-reflector deposition, a-Si alloy deposition, transparent conducting oxide deposition, and module assembly, was optimized for the production of high-efficiency stable modules in a high yield. The improvements that resulted in Task 1 & Task 2 were incorporated to improve the performance of solar cell.

We have systematically investigated the dependence of sub-cell efficiency on the thickness of each layer and current matching. The short circuit current densities of the component cells were, for example, 6.6/6.8/7.2 mA/cm^2 for the top, middle and the bottom component cell as we see from the Quantum efficiency curve in Figure 11. We explored the effect of different current mismatching conditions on the efficiency by adjusting the thickness of i1, i2 and i3 layers.

When the i3 was thinner, Jsc decreased. However, the fill-factor increased at the same time because the current limiting thin top cell had a higher fill-factor and also mismatched cells have a higher fill-factor. In addition, the top-cell limited devices had a better stability because the thinner top-cell was more stable. Therefore, we designed the device to be top-cell limited. The i1 layer was designed to have the highest current since it is the component cell with a relatively low fill-factor. Since EVA/Tefzel encapsulation absorbs some light, we produced the top i layer (i3) slightly thicker to compensate the current loss due to EVA absorption and still maintain the proper current matching.

Besides optimizing all three i layers, we also studied and adjusted the deposition conditions of all n^+ and p^+ layers to achieve the following:

- to have enough doping and thickness to maintain high Voc;
- to maintain minimal thickness to reduce the absorption. This is especially important for the p3 layer.
- to make good tunnel junction between p1 and n2 and between p2 and n3 layers;
- to reduce series resistance.

Each of the nine layers was optimized under the production condition of 1 ft/min.

We have achieved sub-cell active area efficiency of 10.23% for 7.35 cm^2 area triple-junction solar cell, as shown in Figure 20. This test cell is processed in our commercial QA/QC process, utilizing screen printing for the TCO scribing and for gridding. Silver paste is used for the grids.

Production uniformity and consistency were evaluated by measuring cell characteristics of QA/AC coupons, shown in Figure 21, taken from the entire length of 2500 ft. production runs.

Table 1 is a summarized computer printout of the J-V of such a coupon. It shows good uniformity. The J-V curve in Figure 20 is a slow quasi static J-V measurement for cell #4 of this coupon. The fill-factor in Table 1 is slightly overestimated due to the fast J-V measurement in a production process. We use FF>=0.55 as the criterion to determine sub-cell yield. Listed at the bottom of Table 1, are the yield and the averages of Voc, Jsc, Pmax (efficiency) and fill-factor for such a coupon.

Table 2 is a summary of coupon averages throughout the entire roll of about 700m. Each line in this table is the average data for a coupon. The averages we obtained for Table 1 from coupon 254 are listed under slab 254 of Table 2, indicating the cell performance around this slab. Slab 17 is the first one with a-Si solar cell deposited on it in this roll. Table 2 demonstrated high uniformity and consistency of our continuous roll-to-roll process.

Optimization of Module Performance

Sub-cell efficiency improvements described in the previous section directly contributed to the improvements of module efficiency. In addition, we improved the module efficiency by reducing the loss in module fabrication and assembly process. The loss in module efficiency is due to the following three factors:

- coverage losses due to TCO etching line, grid line and bus bars;
- electrical losses due to the resistivity of the TCO, grid lines and bus bars.
- current loss due to encapsulation

We used computer modeling to calculate the losses from different aspects. We then redesigned the artwork for the etching line, grid line and bus bars. The newly designed artwork reduces the loss in module assembly from the previous 17% to the current 13%. We replaced the conductive tape bus bar with thin wire and reduced both the coverage and the electrical loss from bus bar at the same time.

During this program period, we have achieved 8.5% initial aperture area efficiency in 1 ft.x 4 ft. modules. Figure 22 is an I-V curve of such a module measured at ECD with a Spire Solar Simulator under standard condition. The initial module power output was measured to be 33.7 W with 8.5% initial efficiency. The I-V curve of the same module was measured at NREL and shown in Figure 23. The NREL measurement showed 34.2 W power output with 8.56% initial efficiency. These data measured at ECD and NREL showed an excellent agreement.

Stability Testing

One of the major goals of this program is to improve the stable module efficiency. Therefore, when we optimize the cell design and deposition conditions, we use the stable efficiency as the final criteria. For this purpose we tested the long term stability of sub-cells and PV modules under one sun condition. In the following we describe the light soaking test results of sub-cells and modules.

We exposed QA/QC coupons under simulated one sun light at approximately 50°C under no load to test the stability. In Table 3 we list the average performance of sub-cells on a coupon. This table shows that the efficiency was stabilized after 500 hours of exposure. The total loss in efficiency after 1200 hours of exposure at 50°C was 20%. We are now further optimizing our deposition process to reduce the loss due to light soaking.

A solar cell module (Module 011) has been light-soaked under simulated one sun at 50°C under no load. In Table 4 we list the module performance at different light soaking time intervals. The final efficiency of this module after 500 hours of light soaking was 7.0%. The loss in the module efficiency due the light soaking was 19%.

Figure 15: Continuous Roll-to-Roll Substrate Washing Machine

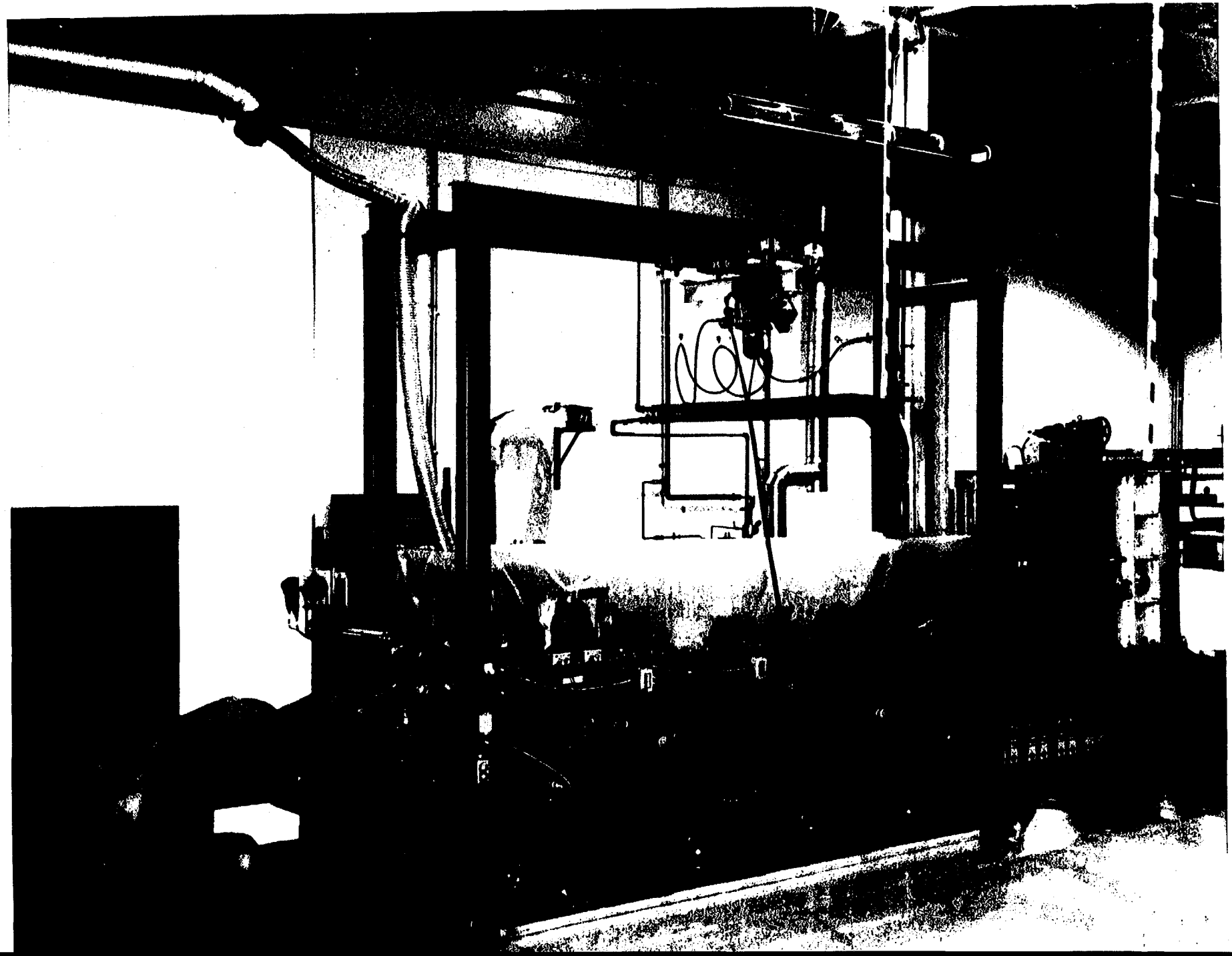

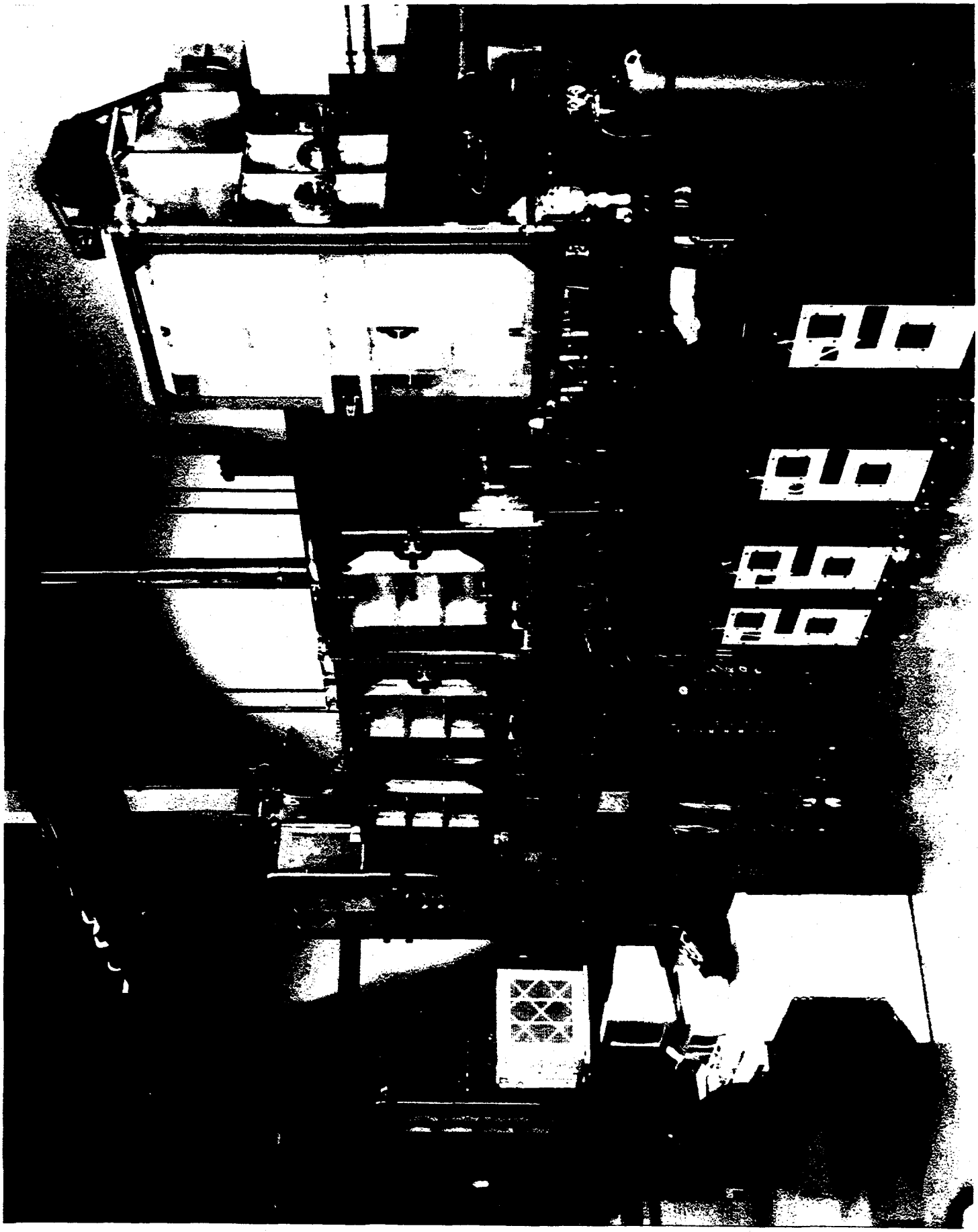

Figure 17: Continuous Roll-to-Roll Amorphous Silicon Alloy Deposition Machine

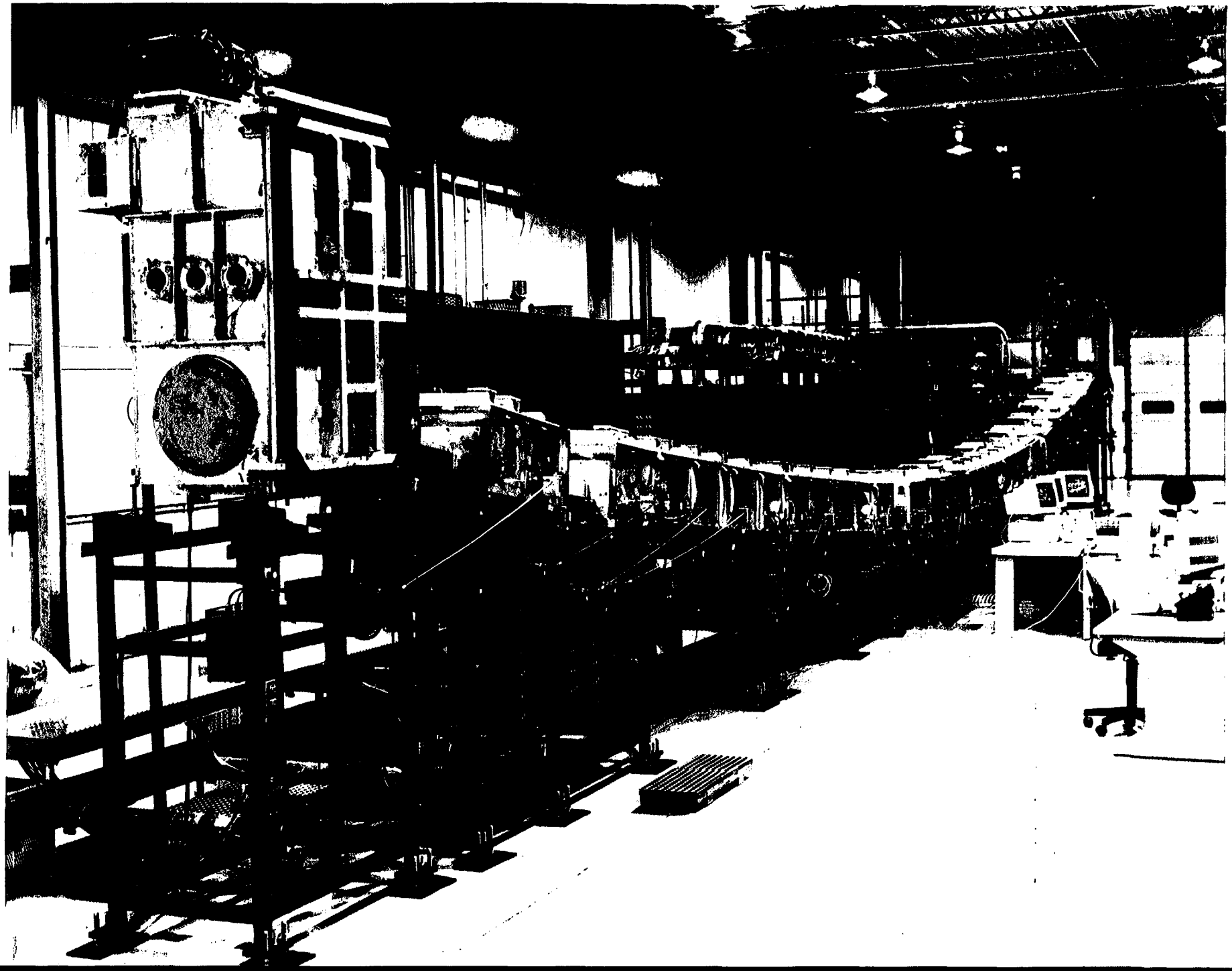

Figure 19: A schematic drawing of 1ft. x 4ft. module.

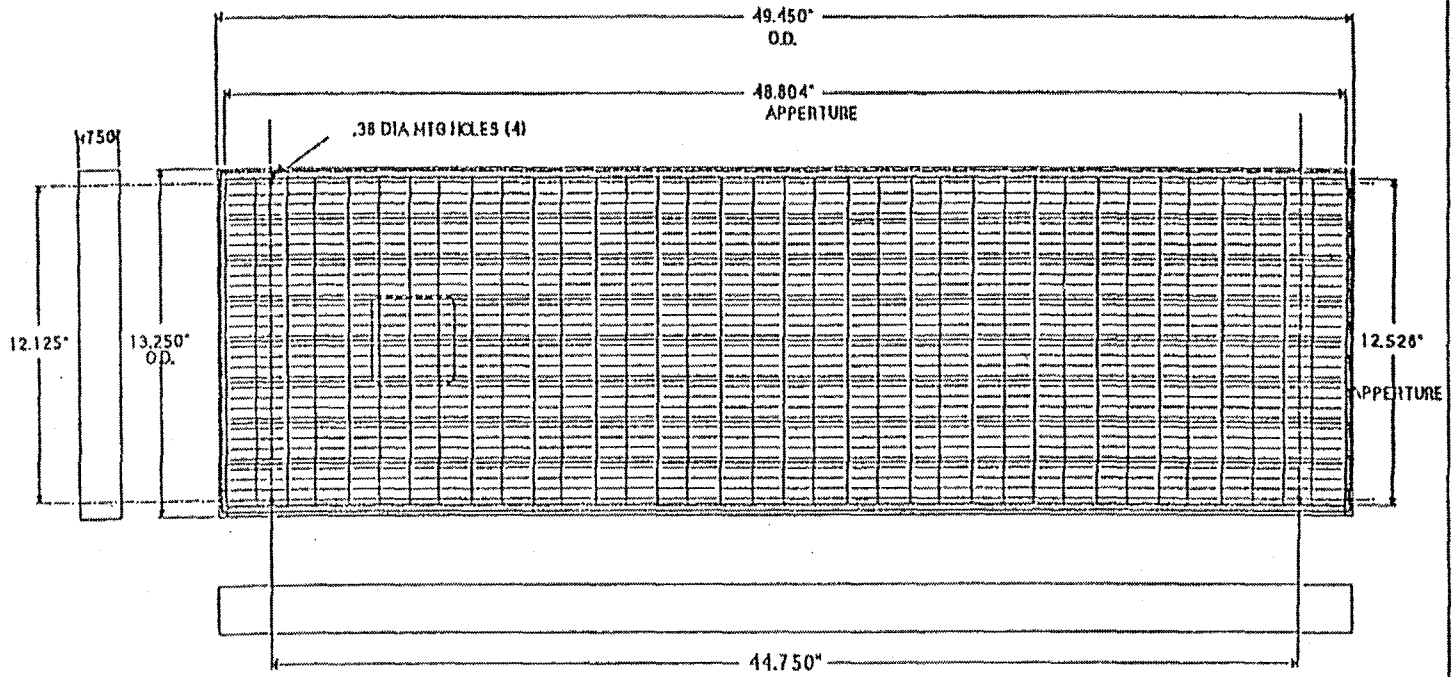

DESIGN REF.

USED ON:

APPR

E C D

Energy Conversion Devices, Inc.
1675 WEST MAPLE ROAD
TROY, MICHIGAN 48084

ECD CONFIDENTIAL

The information contained herein is proprietary to Energy Conversion Devices Inc., Troy, Michigan, (ECD), and shall not be reproduced, used or disclosed in anyway except as approved in writing by an authorized representative of ECD.

THIRD ANGLE PROJECTION

MM (INCH)

25.4 MM = 1 INCH

TOLERANCES EXCEPT AS NOTED

ANGLES:

MM	INCHES
0 ±	0 ±
.0 ±	.00 ±
.00 ±	.000 ±

INTERPRET THIS DRAWING PER ANSI Y14.5-1973

MAXIMUM SURFACE ROUGHNESS EXCEPT AS NOTED

REMOVE BURRS & SHARP EDGES EXCEPT AS NOTED

MATERIAL

FINISH

E C D

DO NOT SCALE DRAWING

DRFT ACD

CHKD

DESIGNER

PROJ ENGR

DATE 10-30-92

SCALE NONE

REDUCTION: NONE

DIVISION MACHINE DIVISION | PROJ NREL

TITLE

OVONIC P2 MODULE DIMENSIONS

SHEET 1 OF

SIZE	DRAWING NO.	REV
D	CAD 102092	A

Figure 20: J-V Curve of a 7.35cm² triple-junction sub-cell.

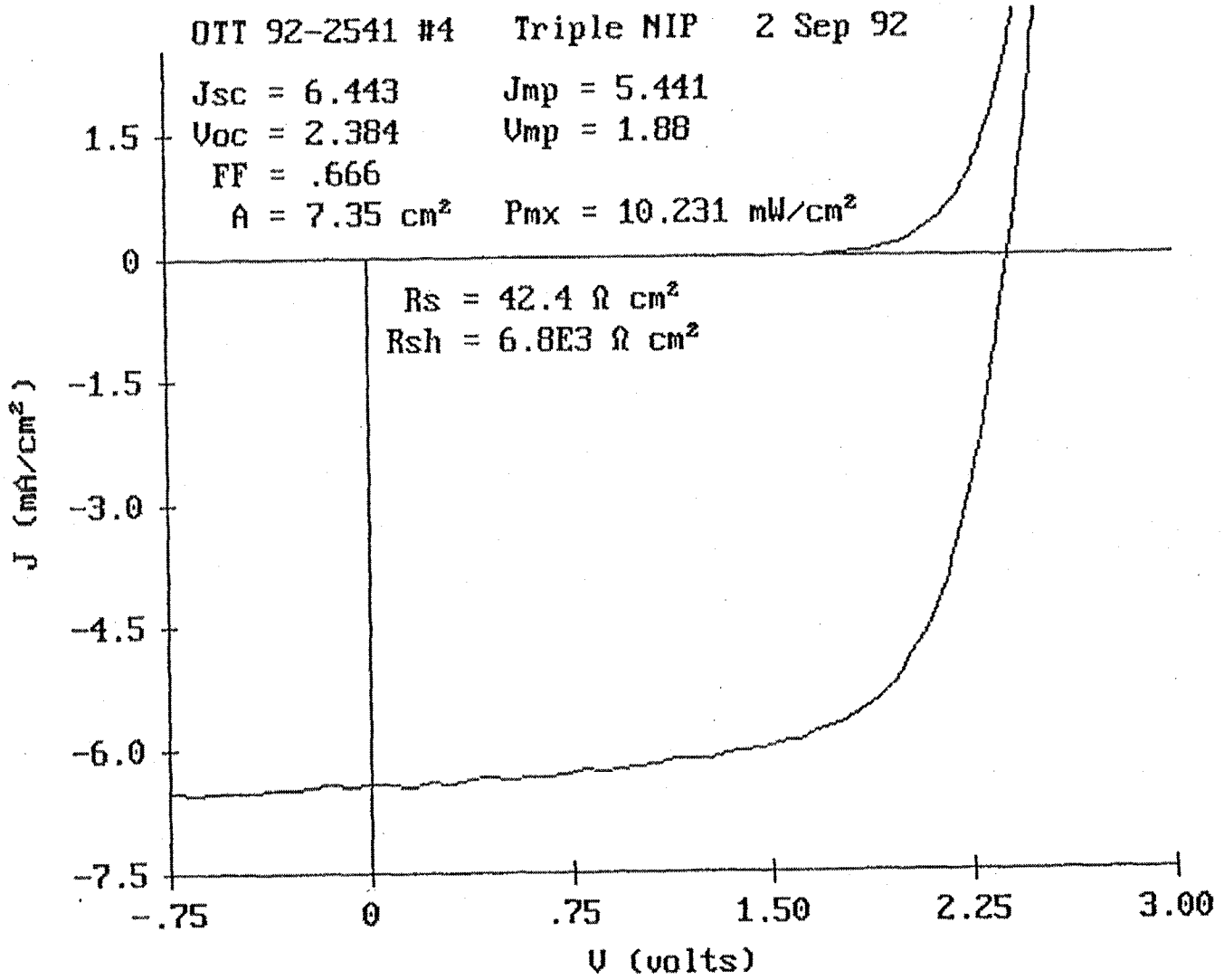

Figure 21: A schematic drawing of a QA/QC coupon with 28 sub-cells. ($7.35cm^2$ active area)

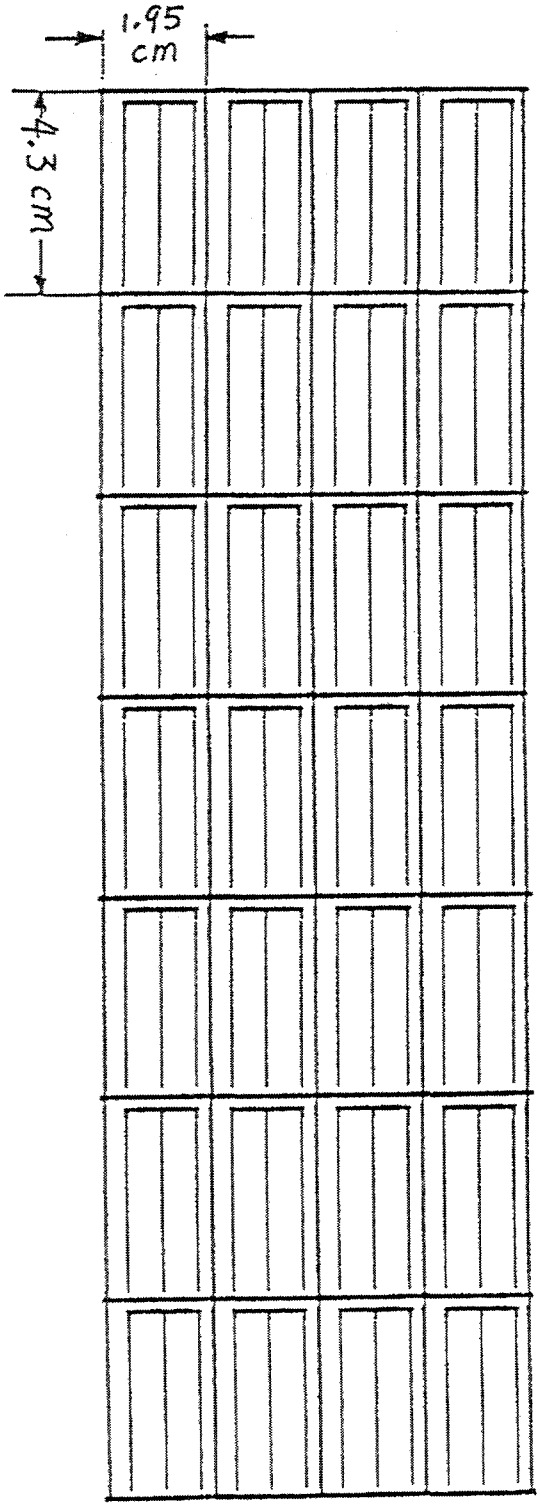

Figure 22: I-V Curve of a 1ft. x 4ft. module measured at ECD.

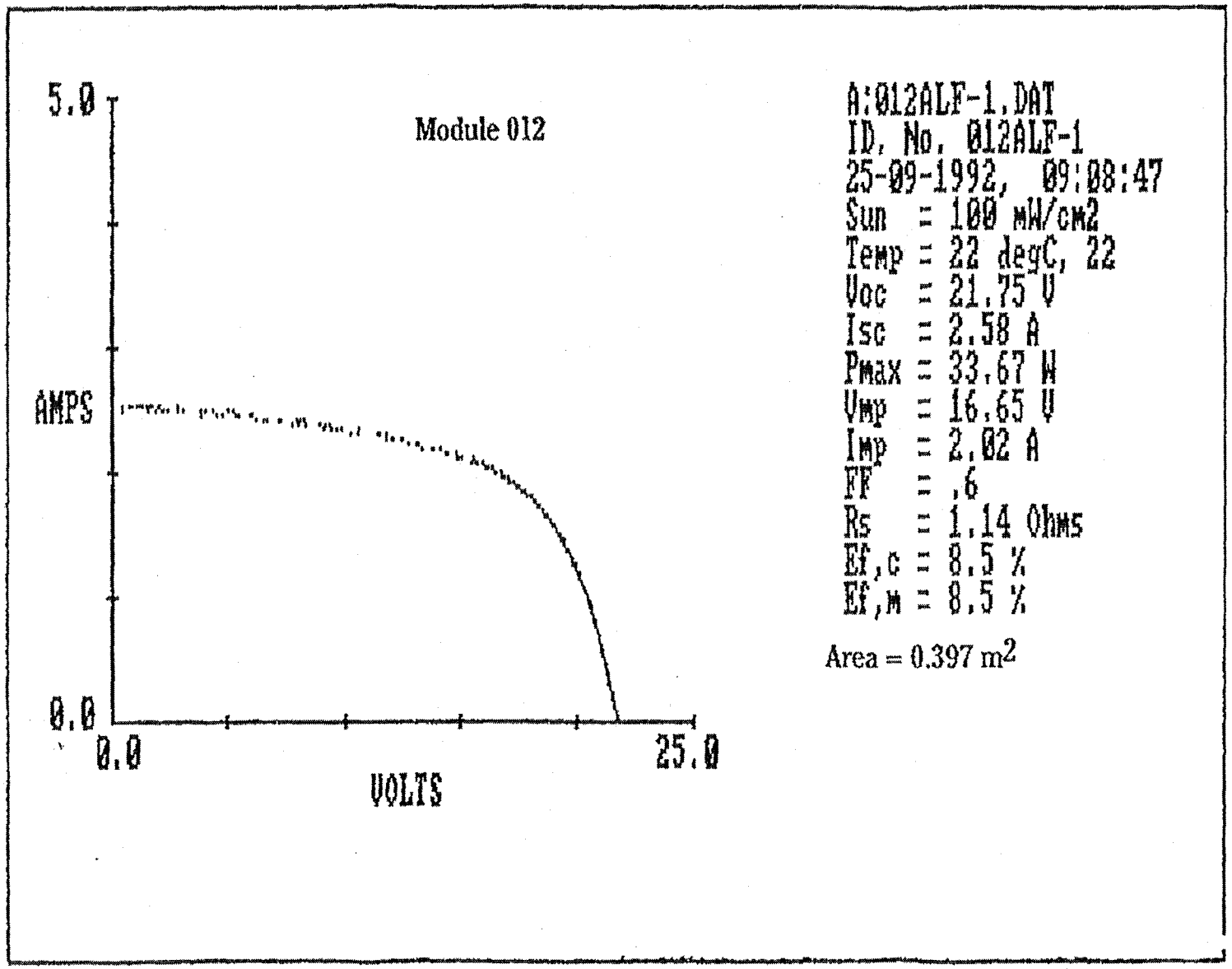

Figure 23: I-V Curve of a 1ft. x 4ft. module measured at NREL.

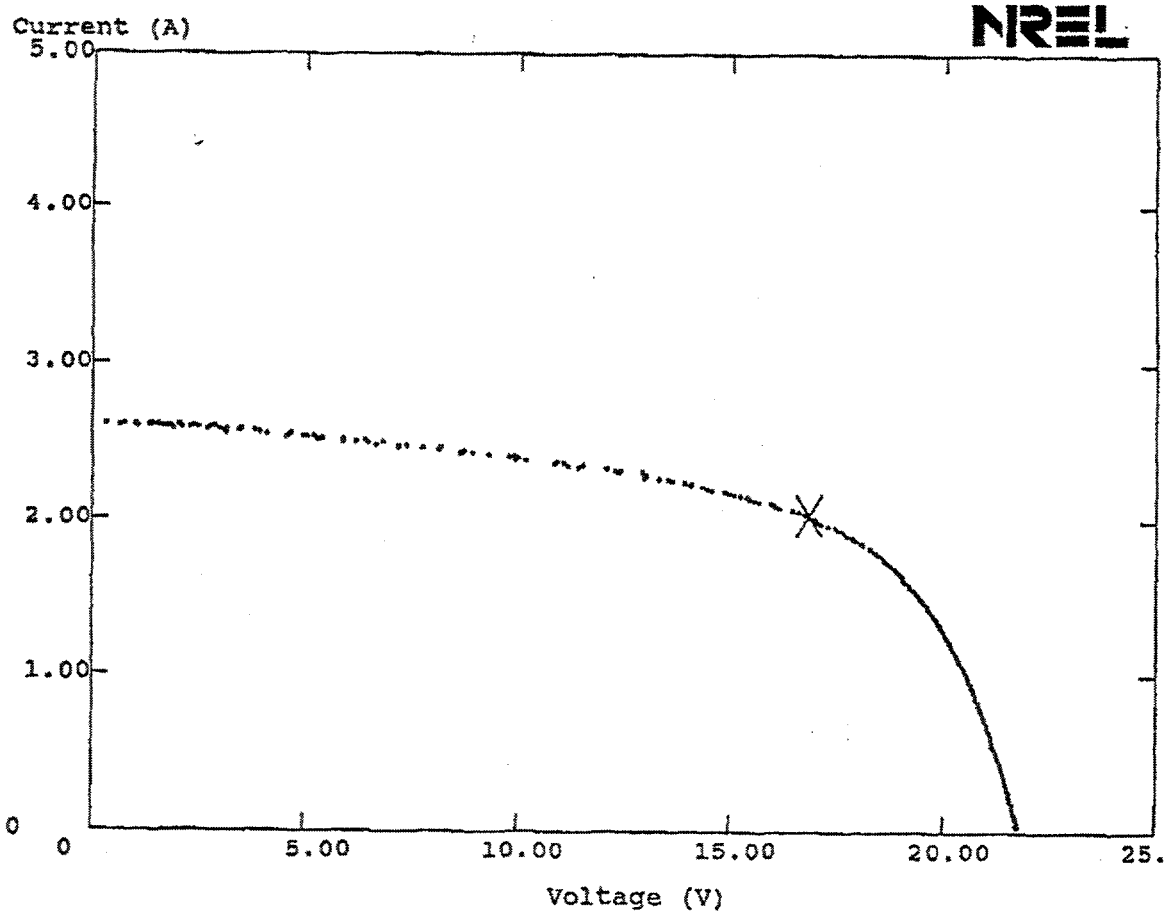

File Name : C:\IV\data\IV3478.xy

Manufacturer: ECD
Sample Type : a-Si/a-Si/a-Si:Ge tandem module
Sample # : 012

Test Date : October 15, 1992
Test Time : 1:18 PM
Spectrum : ASTM E892 Global
SERI SPIRE 240A solar simulator
Estimated total uncertainty in efficiency is ±10 %

Total irradiance = 1000 W/m^2
Temperature = 25 °C
Aperature Area = 3997 cm^2

Voc = 21.79 V
Isc = 2.610 A
Pmax = 34.21 W
V at Pmax = 16.84 V
I at Pmax = 2.031 A
Fill Factor = 60.2 %
Efficiency = 8.56 %

Table 1: Statistical data for J-V curves of 28 cells on a QA/QC coupon.

```
1 pmax =10.05  vmp = 1.95  jmp = 5.15  jsc = 6.01  voc = 2.38  FF = 0.704
2 pmax =10.17  vmp = 1.82  jmp = 5.60  jsc = 5.99  voc = 2.37  FF = 0.717
3 pmax =10.38  vmp = 1.85  jmp = 5.60  jsc = 6.36  voc = 2.37  FF = 0.689
4 pmax =10.66  vmp = 1.77  jmp = 6.02  jsc = 6.52  voc = 2.38  FF = 0.688
5 pmax =10.39  vmp = 1.88  jmp = 5.53  jsc = 6.25  voc = 2.36  FF = 0.705
6 pmax =10.19  vmp = 1.98  jmp = 5.16  jsc = 6.25  voc = 2.37  FF = 0.689
7 pmax =10.14  vmp = 1.90  jmp = 5.34  jsc = 6.46  voc = 2.38  FF = 0.660
8 pmax = 9.85  vmp = 1.78  jmp = 5.54  jsc = 6.13  voc = 2.37  FF = 0.679
9 pmax =10.14  vmp = 1.98  jmp = 5.14  jsc = 6.08  voc = 2.37  FF = 0.704
0 pmax =10.46  vmp = 1.85  jmp = 5.65  jsc = 6.29  voc = 2.38  FF = 0.700
1 pmax =10.48  vmp = 1.89  jmp = 5.54  jsc = 6.28  voc = 2.38  FF = 0.701
2 pmax =10.10  vmp = 1.81  jmp = 5.58  jsc = 6.24  voc = 2.35  FF = 0.690
3 pmax =10.10  vmp = 1.88  jmp = 5.38  jsc = 6.11  voc = 2.37  FF = 0.697
4 pmax =10.07  vmp = 1.89  jmp = 5.32  jsc = 6.11  voc = 2.37  FF = 0.696
5 pmax =10.09  vmp = 1.96  jmp = 5.14  jsc = 5.92  voc = 2.38  FF = 0.716
6 pmax =10.49  vmp = 1.88  jmp = 5.59  jsc = 6.43  voc = 2.37  FF = 0.689
7 pmax =10.00  vmp = 1.92  jmp = 5.21  jsc = 6.09  voc = 2.37  FF = 0.694
8 pmax =10.86  vmp = 1.96  jmp = 5.53  jsc = 6.49  voc = 2.38  FF = 0.704
9 pmax =10.13  vmp = 1.81  jmp = 5.60  jsc = 6.29  voc = 2.36  FF = 0.683
0 pmax = 7.82  vmp = 1.65  jmp = 4.74  jsc = 6.36  voc = 2.23  FF = 0.552
1 pmax = 9.86  vmp = 1.85  jmp = 5.32  jsc = 6.13  voc = 2.37  FF = 0.680
2 pmax =10.04  vmp = 1.88  jmp = 5.32  jsc = 6.18  voc = 2.37  FF = 0.686
3 pmax =10.02  vmp = 1.88  jmp = 5.32  jsc = 6.18  voc = 2.37  FF = 0.685
4 pmax =10.04  vmp = 1.88  jmp = 5.35  jsc = 6.24  voc = 2.37  FF = 0.679
5 pmax =10.52  vmp = 1.90  jmp = 5.54  jsc = 6.46  voc = 2.38  FF = 0.684
6 pmax =10.36  vmp = 1.83  jmp = 5.67  jsc = 6.42  voc = 2.37  FF = 0.682
7 pmax =10.35  vmp = 1.93  jmp = 5.37  jsc = 6.24  voc = 2.36  FF = 0.703
8 pmax = 9.81  vmp = 1.80  jmp = 5.46  jsc = 5.88  voc = 2.38  FF = 0.701

est Cell #  18              Voc  2.38     Jsc 6.48      FF .704
max 10.85    Eff (%) 10.85

FOR CELLS  WITH FF > 0.55
ield  100 %  Voc(avg)  2.36              Isc(avg)  6.22
m(avg)  10.12              FF(avg)  .687


UN # 092   COUPON #  2541   Date 08-31-1992   Time 09:58:18
```

Table 2: Average cell performance data of coupons throughout an entire run.

SLAB #	Voc (V)	Jsc (mA/cm^2)	FF	Eff (%)	YIELD (%)
17	2.29	6.06	0.64	8.89	100
21	2.3	6.17	0.65	9.31	100
25	2.3	6.1	0.66	9.36	93
29	2.29	6.07	0.66	9.15	100
33	2.31	6.07	0.67	9.38	96
37	2.28	6.07	0.63	8.76	93
41	2.26	5.9	0.56	7.55	11
45	2.33	6.1	0.65	9.31	96
49	2.29	5.97	0.65	8.86	96
50	2.31	5.92	0.66	9.09	96
53	2.29	6.04	0.65	8.99	100
57	2.33	6.11	0.66	9.46	96
61	2.29	5.89	0.63	8.58	61
65	2.31	6.02	0.66	9.14	82
69	2.3	5.93	0.64	8.74	96
73	2.28	6.06	0.66	9.13	82
77	2.29	5.82	0.62	8.29	54
81	2.29	6.18	0.67	9.54	93
85	2.31	6.05	0.66	9.3	96
89	2.32	6.04	0.67	9.41	93
90	2.3	6.17	0.67	9.51	89
94	2.31	5.93	0.67	9.22	96
98	2.3	6.17	0.68	9.61	100
100	2.32	5.97	0.66	9.15	100
102	2.32	5.97	0.66	9.16	93
106	2.29	6.19	0.66	9.31	100
110	2.31	6.01	0.66	9.15	93
114	2.29	6.19	0.68	9.72	100
118	2.32	6.08	0.67	9.54	89
122	2.33	6.24	0.69	10.05	96
126	2.32	6.13	0.68	9.73	89
130	2.29	6.15	0.68	9.53	96
134	2.34	6.08	0.68	9.74	96
138	2.3	6.22	0.69	9.84	96
142	2.33	6.11	0.67	9.62	96
146	2.31	6.27	0.68	9.91	100
150	2.32	6.03	0.67	9.36	100
154	2.29	6.16	0.67	9.42	86
158	2.33	6.17	0.69	9.95	96
162	2.3	6.12	0.68	9.65	82
166	2.33	6.09	0.68	9.7	100
170	2.31	6.24	0.67	9.7	82
174	2.35	6.17	0.68	9.9	100
178	2.3	6.14	0.67	9.44	100
182	2.33	6.13	0.69	9.81	96
186	2.31	6.27	0.68	9.93	100
190	2.34	6.2	0.68	9.85	96
194	2.3	6.26	0.69	9.94	96
198	2.36	6.24	0.68	10.07	100
200	2.34	6.23	0.68	9.88	100
202	2.31	6.18	0.68	9.77	100
206	2.36	6.27	0.67	10	96
210	2.33	6.07	0.67	9.54	100
214	2.33	6.21	0.68	9.92	100
218	2.3	6.29	0.68	9.87	93
222	2.33	6.3	0.68	10.02	89
226	2.32	6.24	0.67	9.76	93
230	2.33	6.2	0.68	9.81	89
234	2.32	6.28	0.69	10.05	100
237	2.34	6.22	0.69	10.06	96
242	2.35	6.26	0.69	10.16	96
246	2.37	6.19	0.69	10.08	96
250	2.32	6.26	0.69	10.04	100
254	2.36	6.22	0.69	10.12	100
258	2.32	6.28	0.68	10	96
262	2.36	6.26	0.68	10.1	100
266	2.33	6.32	0.69	10.17	96
270	2.36	6.32	0.69	10.27	100
274	2.31	6.26	0.69	10.05	100

Table 2: Average cell performance data of coupons throughout an entire run. (continued)

SLAB #	Voc (V)	Jsc (mA/cm^2)	FF	Eff (%)	YIELD (%)
278	2.35	6.34	0.69	10.35	100
282	2.32	6.33	0.69	10.18	100
286	2.37	6.26	0.69	10.18	96
290	2.32	6.26	0.70	10.09	100
294	2.35	6.26	0.69	10.17	96
298	2.32	6.61	0.67	10.29	93
300	2.34	6.14	0.69	9.96	100
302	2.36	6.24	0.69	10.24	96
306	2.32	6.68	0.67	10.36	100
310	2.36	6.26	0.69	10.26	100
314	2.32	6.92	0.65	10.45	93
318	2.36	6.27	0.69	10.21	100
322	2.32	6.18	0.69	9.95	100
326	2.36	6.17	0.70	10.16	96
330	2.33	6.17	0.70	10.06	93
334	2.35	6.18	0.70	10.11	100
338	2.32	6.19	0.69	9.93	96
342	2.37	6.16	0.67	9.87	82
346	2.32	6.11	0.69	9.75	100
350	2.34	6.11	0.69	9.93	93
354	2.31	6.13	0.69	9.83	96
358	2.37	6.19	0.69	10.14	96
362	2.33	6.13	0.69	9.91	96
366	2.37	6.08	0.68	9.79	96
379	2.37	6.16	0.69	10.02	96
380	2.36	4.45	0.69	7.21	100
381	2.37	6.15	0.69	10.08	96
382	2.37	6.1	0.69	10.04	93
383	2.37	6.11	0.68	9.94	100
384	2.37	5.99	0.68	9.59	93
385	2.38	6.06	0.69	9.91	93
386	2.36	6.1	0.68	9.85	100
387	2.37	6.21	0.67	9.91	100
388	2.37	5.99	0.68	9.74	100
389	2.37	6.15	0.68	9.96	96
390	2.36	6.06	0.69	9.91	96
407	2.35	6.26	0.69	10.21	100
408	2.35	6.21	0.69	10.05	100
409	2.35	6.2	0.68	9.88	100
413	2.36	5.88	0.70	9.66	100
414	2.37	5.92	0.70	9.88	100
415	2.35	6.02	0.70	9.87	100
419	2.32	6.26	0.68	9.86	100
421	2.33	6.18	0.68	9.72	100
STD DEV	0.027	0.218	0.019	0.517	10.529
AVG	2.329	6.145	0.676	9.707	94.971

Table 3: Light soaking test data of triple-junction sub-cells of 7.35cm^2 size.

Light Soaking Time(Hours)	VOC (V)	JSC (mA/cm2)	FF	Efficiency (%)	Drop in Efficiency (%)
0 (INITIAL)	2.323	6.33	0.66	9.72	
24	2.24	6.27	0.61	8.56	12
144	2.243	6.23	0.59	8.23	15
500	2.231	6.09	0.58	7.81	20
1240	2.195	6.15	0.57	7.74	20

Table 4: Light soaking test data of a triple-junction module.

Light Soaking Time(Hours)	Voc (V)	Isc (A)	FF	Pmax (W)	Efficiency (%)	Drop in Efficiency (%)
0 (INITIAL)	11.93	2.59	0.61	18.75	8.6	
25	11.55	2.5	0.56	16.18	7.4	14
70	11.52	2.46	0.56	15.75	7.2	16
250	11.54	2.46	0.55	15.76	7.2	16
500	11.45	2.45	0.54	15.25	7	19

Task 4: Incorporating Microwave Plasma CVD Manufacturing Technology

In this section of the report, we discuss the progress made in the large-area high-rate deposition of intrinsic hydrogenated amorphous silicon, using a "microwave linear applicator". Our work has concentrated in two principal areas: (1) achieving uniform depositions over a large area; (2) materials characterization.

Deposition uniformity by any technique is controlled by two factors, the uniformity of the applied energy, and the uniformity of the "applied" reactant gas mixture. Applying the energy uniformly in radio frequency (rf) plasma enhanced chemical vapor deposition (rf-PECVD) systems is usually not a fundamental problem because at those rf frequencies (typically 13.56 MHz), the wavelength (22m) far exceeds the dimensions of even large (~1m) cathodes used in industrial applications. Therefore, it is the reactant gas flow pattern which actually governs the deposition uniformity. Since we are presently using a gas manifold that is similar to those in our rf-systems, we do not expect the uniformity to be affected by the gas flow. In microwave PECVD (mw-PECVD) on the other hand, the wavelength can be smaller than the substrate dimensions. For example, at 2.45 GHz, the wavelength is only 12.25cm (~5 inches). For substrates on the order of 15 inches, this can present serious difficulties.

The solution to the uniformity problem is to "broadcast" the microwave energy evenly over the desired area. In this way, mw-PECVD more resembles photo assisted CVD where deposition uniformity depends on the uniformity of the photon beam. The result of more effectively confining the microwave radiation by proper use of reflecting surfaces is shown in comparison of Figure 24 (a) and (b). In that figure, we show the thickness variation of the central region of the deposition pattern for two films. The data shows three things: (1) the thickness uniformity (+/- 10%) increased from about 5 inches in (a) to about 8 inches in (b); (2) a shift of the thickness maximum toward the center of the Applicator; and (3) an increase in the deposition rate from about 2nm/s to about 5nm/s (while using less microwave power).

Continued work on the Applicator design has shown that in subsequent runs, the peak position of the deposition is now located at about the 7 in. position, i.e., within about a 1/2 in. of the center of the Applicator, see Figure 24. This improvement was a result of eliminating "stray" radiation. Radiation leaking out from the connection between the Applicator and the microwave feed-through had contributed to the radiation emitted from the Applicator itself. Thus the plasma at one end of the Applicator was more intense than at the other, resulting in the skewed deposition patterns shown in Figure 24.

We have characterized the films deposited on 7059 glass by infrared (ir) and Raman spectroscopies, by their electrical response including their dark and photo conductivities and also their activation energies, as well as by their density of defect states measured by the photothermal deflection spectroscopic (PDS) technique.

Figure 25 shows the ir spectrum of a sample. We show in Figure 25 (a) the SiH stretching absorption band, and in Figure 25 (b), we show the bending bands. The film is about 1.8

um thick for a deposition rate of about 3 nm/s and was deposited on a crystalline substrate. The figure shows that in addition to the monohydride (SiH) groups, the film contains some dihydride (SiH_2) bonding groups as shown by the spectral features at 2090 cm^{-1} and 890 cm^{-1}, in the stretching and bending regions, respectively, of the spectra. The total bonded hydrogen concentration was determined by integrating over the SiH bending band centered near 640 cm^{-1} according to:

$$[H] = 1.6 \times 10^{19} \int (\alpha/\omega) d\omega,$$

and the absorption coefficient by the expression

$$\alpha = A/ (t \log_{10} e),$$

where A is the absorbency, and t the film thickness. We find that [H] is 9.2 atom %.

The Raman spectrum was taken and we find that the peak position of the dominant TO band is about 483 cm^{-1} with a full width of 67 cm^{-1}. These values, i.e., a relatively narrow peak near 480cm^{-1}, indicate a well-relaxed structure.

Measuring the temperature dependence of the electrical conductivity, we find that Ea = 0.80 eV and $\sigma_o = 3550\ (\Omega cm)^{-1}$. The dark and photo conductivity's (measured under approximately 300mW/cm^2) are $\sigma_d = 4.2 \times 10^{-9}\ (\Omega cm)^{-1}$ and $\sigma_p = 1.2 \times 10^{-4}\ (\Omega cm)^{-1}$, respectively. Thus the sample has a high absolute photo conductivity as well as a high ratio (σ_p/σ_d) of about 4.5 orders of magnitude.

The PDS result for the sample is shown in Figure 26. We estimate that the defect density is 1.2×10^{16} cm^{-3} for an a-Si:H film deposited at 3 nm/s.

We have begun to evaluate these intrinsic films in p-i-n solar cell devices. The p and n layers were deposited in a load locked rf deposition system. In addition, thin intrinsic buffer layers were deposited in the rf system, rf-(i), before and after the intrinsic layer that was deposited by the microwave system, mw-(i).

Figure 24: Deposition uniformity along length of applicator.

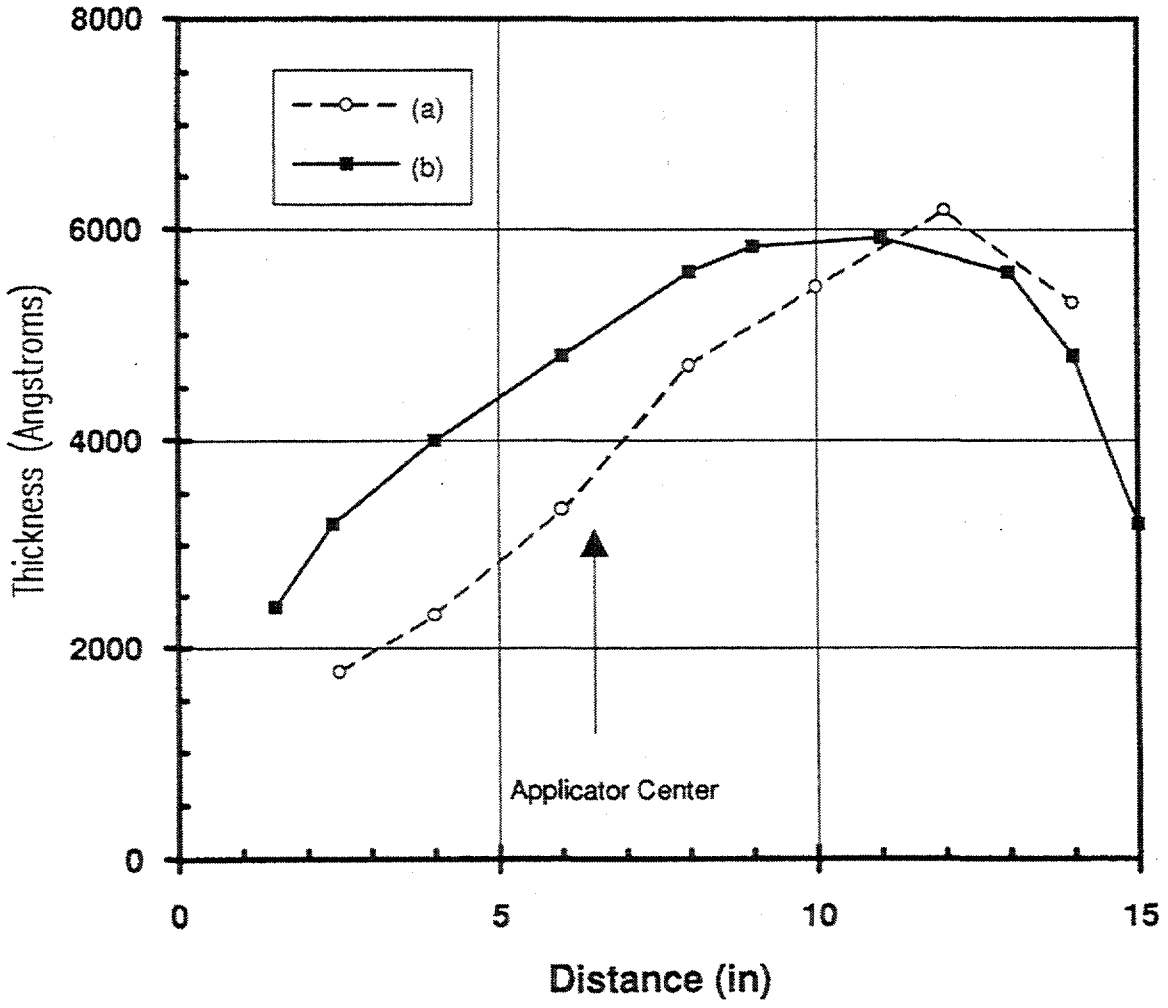

Figure 25: Infra-red absorbance spectrum of a sample deposited with the high rate microwave linear applicator.
(a) Stretching band of Silicon Hydride
(b) Bending band of Silicon Hydride

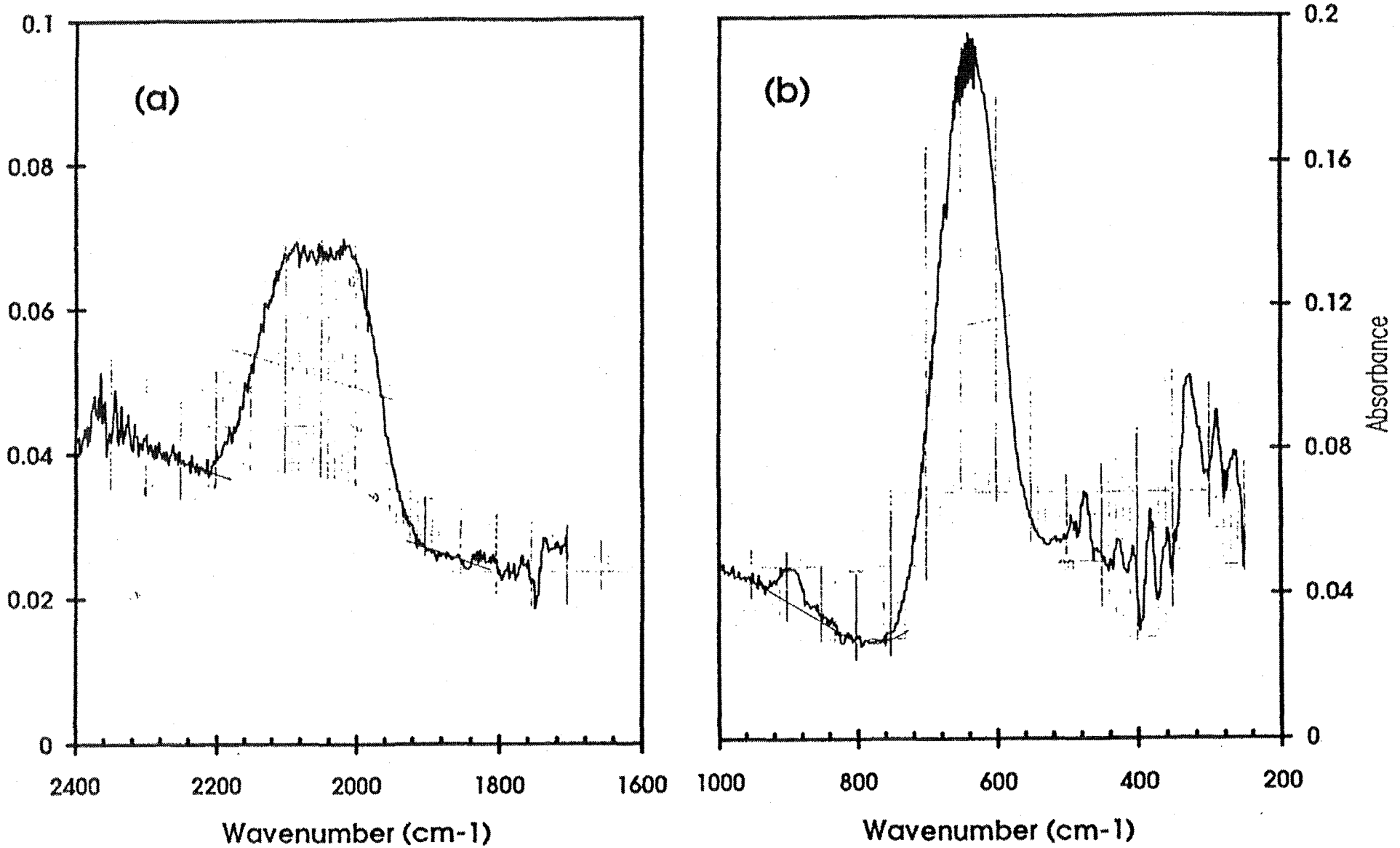

Figure 26: PDS spectrum of a high deposit rate microwave deposited sample.

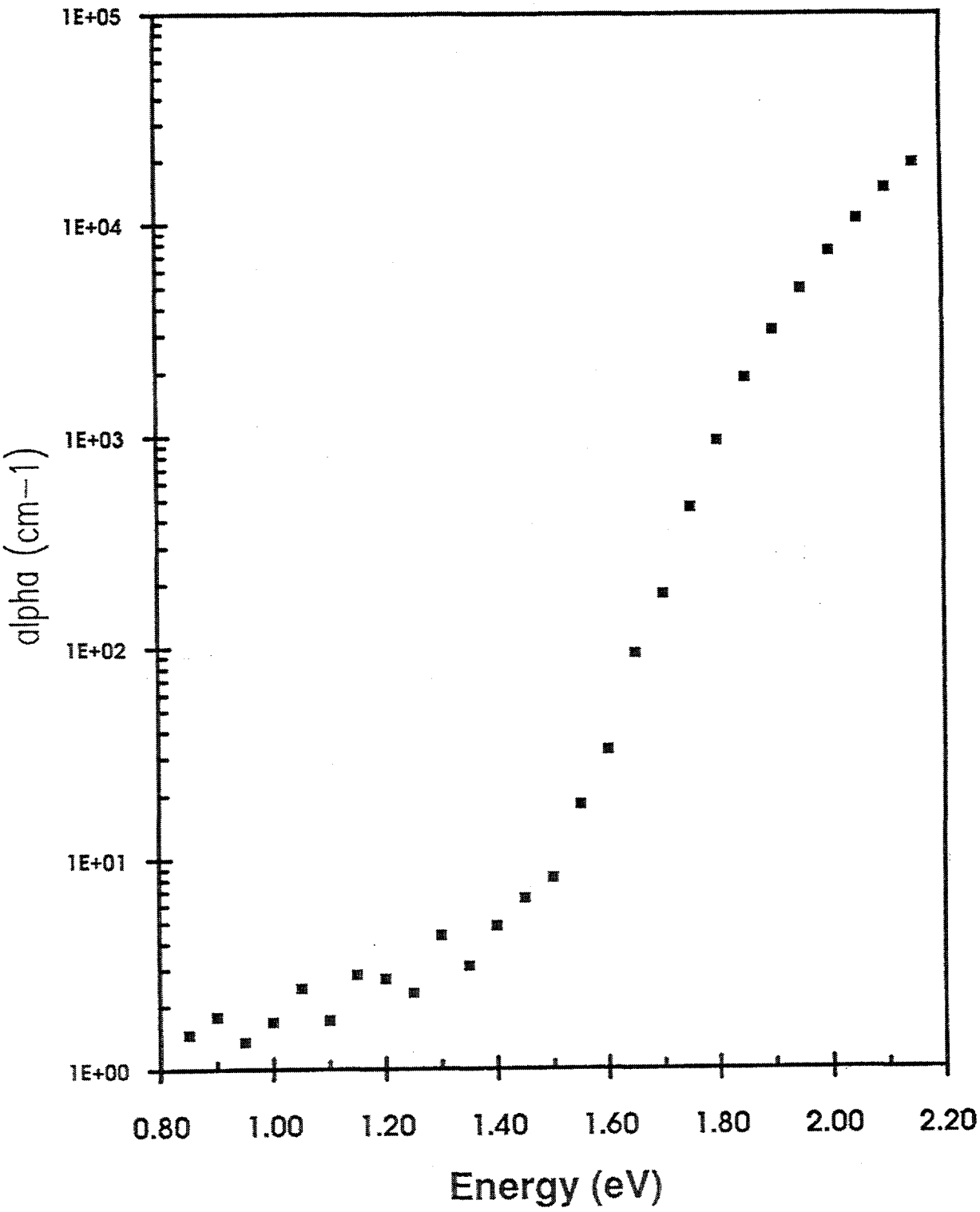

TASK 5: MATERIAL COST REDUCTION

One of the highest cost items in the bills of materials for ECD's triple-junction multiple band-gap a-Si alloy solar cell consisting of Si/Si/Si-Ge structure is germane and disilane. In this program period, efforts were made to determine long term price projections for these gases. We have identified Mitsui Toatsu and Voltaic as the world largest manufacturers for disilane and germane gases, respectively. Germane and disilane gases used in this program were supplied by these companies. The prices were substantially lower than the current world prices due to contracted large volume purchase. We also worked with our Russian joint venture partner, Sovlux, to achieve cost reductions for these gases. We have obtained disilane and germane gases produced in Russia. The results of purity analyses of these gases indicated that germane had acceptable purity, whereas disilane had unacceptable high levels of impurities. The material cost factors for these gases have been significantly reduced due to the thickness reduction of the Si-Ge narrow band-gap solar cells as the result of optimization of solar cell structure and deposition conditions. A concept for a new module design to reduce material costs have been developed.

References

1 Production of Tandem Amorphous silicon Alloy Cells in a Continuous Roll-to-Roll Process, M. Izu and S. R. Ovshinsky, SPIE Proc. 407, 42 (1983).

2 Roll-to-Roll Plasma Deposition Machine for the Production of Tandem Amorphous Silicon Alloy Solar Cells, M. Izu and S. R. Ovhsinsky, Thin Solid Films 119 55 (1984).

3 Amorphous Silicon Solar Cells Production in a Roll-to-Roll Plasma CVD Process, H. Morimoto and M. Izu, JARECT 16 (1984); Amorphous Semiconductor Technology & Devices, North Holland Publishing Company, Edited by Y. Hamakawa, 212 (1984).

4 Roll-to-Roll Mass Production Process for Amorphous Silicon Solar Cell Fabrication, S. R. Ovshinsky, Proc. International PVSEC-1, 577 (1988).

5 High Efficiency Multiple-Junction Solar Cells Using Amorphous Silicon and Amorphous Silicon-Germanium Alloys, J. Yang, R. Ross, T. Glatfelter, R. Mohr, G. Hammond, C. Bernotaitis, E. Chen, J. Burdick, M. Hopson and S. Guha, Proc. 20th IEEE P.V. Spec. Conf. 241 (1988).

6 Physics of High Efficiency Multiple-Junction Solar Cells, J. Yang, R. Ross, R. Mohr and J. P. Fournier, Proc. MRS Symp. Vol. 95, 517 (1987).

7 Performance of Large Area Amorphous Silicon Based Single and Multiple-Junction Solar Cells, P. Nath and M. Izu, Proc. of the 18th IEEE Photovoltaic Specialists Conf., Las Vegas, Nevada, 939 (1985).

8 1MW Amorphous Silicon Thin-Film PV Manufacturing Plant, P. Nath, K. Hoffman, J. Call, C. Vogeli, M. Izu and S. R. Ovshinsky, Proc. of the 3rd International Photovoltaic Science and Engineering Conf., Tokyo, Japan, 395 (1987).

9 Conversion Process for Passivation Current Shunting Paths in Amorphous Silicon Alloy Solar Cells, P. Nath, K. Hoffman, C. Vogeli and S. R. Ovshinsky, Appl. Phys. Lett. 53 (11), 986 (1988).

10 Yield and Performance of Amorphous Silicon Based Solar Cells Using Roll-to-Roll Deposition, P. Nath, K. Hoffman, J. Call, G. Didio, C. Vogeli and S. R. Ovshinsky, Proc. 20th IEEE P.V. Spec. Conf., 293 (1988).

11 A New Inexpensive Thin Film Power Module, P. Nath, K. Hoffman, C. Vogeli, K. Whelan and S. R. Ovshinsky, Proc. 20th IEEE P.V. Spec. Conf., 1315 (1988).

12 Fabrication and Performance of Amorphous Silicon Based Tandem Photovoltaic Devices and Modules, P. Nath, K. Hoffman and S. R. Ovshinsky, 4th International P.V. Science and Engineering Conf., Sydney, Australia, (1989).

13 Advances in High-Efficiency, Multiple-Band-Gap, Multiple-Junction Amorphous Silicon Based Alloy Thin-Film Solar Cells, S. Guha, A Paper Presented at MRS Spring Meeting, San Diego, April (1989).

14 Amorphous Silicon-Germanium Alloy Solar Cells with Profiled Band-Gaps, J. Yang, R. Ross, T. Glatfelter, R. Mohr and S. Guha, MRS Symposium Proc. Vol. 149, 435 (1989).

15 Low-Pressure Microwave PECVD Technology, M. Izu, S. J. Hudgens, J. Doehler and B. Dotter, Proc. 4th International Conf. on Vacuum Web Coating, 129 (1990).

16 High Deposition Rate Amorphous Silicon Alloy Xerographic Photoreceptor, S. J. Hudgens and A. J. Johncock, Proc. MRS Symp. Vol. 49, 403 (1985).

17 Amorphous Semiconductors for Microelectronics, S. J. Hudgens, Proc. SPIE Vol. 617, 95 (1986).

Document Control Page	1. NREL Report No. NREL/TP-411-5453	2. NTIS Accession No. DE93010006	3. Recipient's Accession No.

4. Title and Subtitle

Continuous Roll-to-Roll a-Si Photovoltaic Manufacturing Technology

5. Publication Date
April 1993

6.

7. Author(s)
M. Izu

8. Performing Organization Rept. No.

9. Performing Organization Name and Address

Energy Conversion Devices
1675 West Maple Road
Troy, Michigan 48084

10. Project/Task/Work Unit No.
PV350101

11. Contract (C) or Grant (G) No.

(C) ZM-2-11040-7

(G)

12. Sponsoring Organization Name and Address
National Renewable Energy Laboratory
1617 Cole Blvd.
Golden, CO 80401-3393

13. Type of Report & Period Covered

Semiannual Technical Report
1 April 1992 - 30 September 1992

14.

15. Supplementary Notes
NREL technical monitor: R. Mitchell

16. Abstract (Limit: 200 words)

This report describes work performed by ECD to advance its roll-to-roll, triple-junction photovoltaic manufacturing technologies; to reduce the module production costs; to increase the stabilized module performance; and to expand the commercial capacity utilizing ECD technology. The 3-year goal is to develop advanced large-scale manufacturing technology incorporating ECD's earlier research advances with the capability of producing modules with stable 11% efficiency at a cost of approximately $1/W_p$. Major efforts during Phase 1 are (1) the optimization of the high-performance back-reflector system, (2) the optimization of a-Si-Ge narrow band-gap solar cell, and (3) the optimization of the stable efficiency of the module. The goal is to achieve a stable 8% efficient 0.3-m x 1.2-m (1-ft x 4-ft) module. Also, the efforts include work on a proprietary, high-deposition-rate, microwave plasma, CVD manufacturing technology; and on the investigation of material cost reduction.

17. Document Analysis
a. Descriptors
amorphous silicon ; manufacturing ; photovoltaics ; solar cells

b. Identifiers/Open-Ended Terms

c. UC Categories
271

18. Availability Statement
National Technical Information Service
U.S. Department of Commerce
5285 Port Royal Road
Springfield, VA 22161

19. No. of Pages
58

20. Price
A04

Form No. 0069E (6-30-87)